

ANALYSIS AND ELIMINATION OF NUMERICAL PRESSURE DEPENDENCY IN COUPLED STOKES-DARCY PROBLEM

JIACHUAN ZHANG

ABSTRACT. This paper presents a pressure-robust mixed finite element method (FEM) for the coupled Stokes-Darcy system. We revisit the rigorous theoretical framework of Layton et al. [2002], where velocity and pressure errors are coupled, masking pressure's influence on velocity accuracy. To investigate the pressure dependency, we introduce an auxiliary velocity projection that preserves discrete divergence and interface continuity constraints. By analyzing the difference between the discrete and projected velocities, we rigorously prove that classical FEM incurs pressure-dependent consistency errors due to inexact divergence enforcement and approximate interface conditions. To eliminate these errors, we design a pressure-robust method using a divergence-free reconstruction operator, which enforces exact divergence constraint and interface continuity. Numerical examples confirm the theory: under high-pressure or low-viscosity, the proposed method reduces velocity errors by orders of magnitude compared to the classical method.

Keywords: pressure-robustness, Stokes-Darcy problem, reconstruction operator, error estimate
Mathematics Subject Classification : 65N15, 65N30, 76D07.

1 Introduction

This paper is concerned with pressure-robust mixed FEMs of the coupled Stokes-Darcy problem. This problem is involved in energy engineering, battery technology, biomedicine, and so on. There are many numerical methods solving this problem [7, 15, 8, 24, 10, 6, 11, 25, 27, 4]. Especially for reference [15], Layton et al. have established a complete theoretical analysis framework for a class of mixed FEMs with respect to two equivalent schemes. However, its convergence analysis is conducted by coupling velocity and pressure together. This makes it unclear how the velocity error depends on pressure.

In this paper, the author revisits the analysis framework proposed in [15] to explore the pressure dependence of velocity error. To overcome the numerous technical difficulties in directly estimating the pressure dependence of $\mathbf{u} - \mathbf{u}_h$, we defined a special projection $S_h \mathbf{u}$ of the velocity field \mathbf{u} onto the discrete solution space V_h , as formulated in equation (3.5). The term $\mathbf{u} - S_h \mathbf{u}$ is pressure-robust and enjoys satisfactory convergence properties. Under this framework, it suffices to explore and compare the pressure dependence of $\mathbf{u}_h - S_h \mathbf{u}$ within the space V_h for classical and pressure-robust methods.

Classical methods relax the divergence constraint and interface normal continuity, and enforce the conditions discretely. Both relaxations will lead to pressure-dependent consistency errors which can potentially pollute the computed velocity. The estimate indicates the pressure-related consistency errors are captured by the following functional:

$$\ell_p(\boldsymbol{\psi}_h) = (\nabla \cdot \boldsymbol{\psi}_h, p) - \langle \boldsymbol{\psi}_h^s \cdot \mathbf{n}^s + \boldsymbol{\psi}_h^d \cdot \mathbf{n}^d, p^d \rangle_\Gamma. \quad (1.1)$$

The pressure dependence arises from the inability to guarantee that $\ell_p(\boldsymbol{\psi}_h)$ always equals zero for $\boldsymbol{\psi}_h \in V_h(0)$. The discrete space $V_h(0)$ consists of functions that satisfy, in discrete sense, divergence-free and interface normal continuity. If these two properties hold exactly, i.e. $\nabla \cdot \boldsymbol{\psi}_h = 0$ and $\boldsymbol{\psi}_h^s \cdot \mathbf{n}^s + \boldsymbol{\psi}_h^d \cdot \mathbf{n}^d = 0$, or the pressure variable comes from the discrete space, i.e. $p \in Q_h$ and $p^d \in \Lambda_h$, the consistency error will vanish. Otherwise, it depends on the pressure and is

School of Physical and Mathematical Sciences, Nanjing Tech University, Nanjing, Jiangsu, 211816, P. R. China. (zhangjc@njtech.edu.cn).

with the estimate

$$\|S_h \mathbf{u} - \mathbf{u}_h\|_X^2 \lesssim \frac{1}{\mu^2} \left(\inf_{\phi_h \in Q_h^s} \|p^s - \phi_h\|_s^2 + h \inf_{\phi_h \in \Lambda_h} \|p^d - \phi_h\|_\Gamma^2 \right) + \|\mathbf{u} - S_h \mathbf{u}\|_X^2.$$

The velocity error demonstrates a positive correlation with measured pressure values while exhibiting an inverse relationship with the fluid viscosity.

For pressure dependence arising from discrete divergence-free constraints, the review article by John et al. [14] systematically examines three methodological frameworks [9, 12, 5, 26, 18, 19]. A notable strategy, firstly proposed in [18], involves implementing divergence-free reconstruction operators exclusively on the right-hand test functions while preserving the original variational formulation on the left-hand side. Remarkably, this relatively straightforward adaptation has demonstrated the capacity to confer pressure robustness when applied to numerous classical numerical schemes [19, 16, 20].

For the Stokes-Darcy coupled problems incorporating discrete divergence-free constraints and discrete interface normal continuity conditions, limited research has been conducted on applying divergence-free reconstruction operators to achieve pressure robustness. To the best of my knowledge, Lv et al. [22] have achieved pressure robustness using reconstruction operators, but their results are limited to the lowest-order FEM. Similarly, Jia et al. [13] developed a pressure-robust weak Galerkin FEM, but only for two-dimensional problem.

Under the framework of $\mathbf{u}_h - S_h \mathbf{u}$ proposed in this paper, the pressure-robust method with reconstruction operator Π_h change the functional (1.1) into

$$\mathfrak{N}_p(\psi_h) = (\nabla \cdot (\Pi_h \psi_h), p) - \langle \Pi_h^s \psi_h^s \cdot \mathbf{n}^s + \Pi_h^d \psi_h^d \cdot \mathbf{n}^d, p^d \rangle_\Gamma. \quad (1.2)$$

If we choose compatible finite element spaces about the approximation spaces and the reconstruction spaces for fluid region and saturated porous medium, then the reconstruction operator will works for removing the pressure dependency related to both discrete divergence-free and discrete interface normal continuity, i.e.

$$\nabla \cdot \Pi_h \psi_h = 0, \quad \text{and} \quad \Pi_h^s \psi_h^s \cdot \mathbf{n}^s + \Pi_h^d \psi_h^d \cdot \mathbf{n}^d = 0.$$

This means the functional shown in (1.2) vanishes (refer to Lemma 4.1). An example of such spaces is that: for the velocity, the approximation space and reconstruction space in the Darcy domain, as well as the reconstruction space in the Stokes domain, all be set Raviart-Thomas (RT) elements with the same order, and the approximation space in the Stokes region is the classical mixed finite element space. With the help of reconstruction operator and setting appropriate finite element spaces, we achieve pressure robustness for the Stokes-Darcy problem with estimate

$$\begin{aligned} \|S_h \mathbf{u} - \mathbf{u}_h\|_X^2 &\lesssim h^2 \sum_{T \in \mathcal{T}_h(\Omega^s)} \inf_{\varphi_h^s \in [P_{k-2}(T)]^N} \|\nabla \cdot D(\mathbf{u}^s) - \varphi_h^s\|_T^2 \\ &\quad + h \sum_{e \in \mathcal{E}_h(\Gamma)} \inf_{q_h \in P_{k-1}(e)} \|D(\mathbf{u}^s) \mathbf{n}^s \cdot \mathbf{n}^s - q_h\|_e^2. \end{aligned}$$

In the numerical aspect, we meticulously designed two cases to compare pressure-robust method with classical method. The first case examines the impact of pressure variations on velocity errors, while the second case investigates the influence of viscosity changes on errors. Both cases also compare the time cost of the two methods. The conclusions obtained fully align with theoretical results and are summarized as follows: For scenarios with either large pressure or small viscosity, the pressure-robust method demonstrates clear superiority over classical method; in other circumstances, both methods perform comparably.

The remainder of this paper is organized as follows. Section 2 presents the Stokes-Darcy coupled system and derives its variational formulation. Section 3 constructs the auxiliary projection $S_h \mathbf{u}$, analyzes the classical mixed FEM discretization, and rigorously characterizes the pressure-dependent velocity error mechanisms. Section 4 proposes a pressure-robust discretization through divergence-free reconstruction operators, eliminating pressure dependence in error

estimates. Section 5 validates theoretical predictions via numerical benchmarks comparing classical and pressure-robust methods under varying pressure and viscosity conditions. Finally, Section 6 summarizes the key findings of this study and outlines potential extensions for future researches.

2 Problem statements and variational formulation

This paper is concerned with pressure-robust FEMs for the Stokes-Darcy problem described by the following systems. The free fluid domain Ω^s and porous media domain Ω^d are governed respectively by:

$$-2\mu\nabla \cdot D(\mathbf{u}^s) + \nabla p^s = \mathbf{f}^s \text{ in } \Omega^s, \quad \nabla \cdot \mathbf{u}^s = g^s \text{ in } \Omega^s, \quad \mathbf{u}^s = 0 \text{ on } \Gamma^s, \quad (2.1)$$

and

$$\mu K^{-1} \mathbf{u}^d + \nabla p^d = \mathbf{f}^d \text{ in } \Omega^d, \quad \nabla \cdot \mathbf{u}^d = g^d \text{ in } \Omega^d, \quad \mathbf{u}^d \cdot \mathbf{n}^d = 0 \text{ on } \Gamma^d, \quad (2.2)$$

with interface conditions on $\Gamma = \Omega^s \cap \Omega^d$:

$$\mathbf{u}^s \cdot \mathbf{n}^s + \mathbf{u}^d \cdot \mathbf{n}^d = 0, \quad (2.3)$$

$$p^s - 2\mu D(\mathbf{u}^s) \mathbf{n}^s \cdot \mathbf{n}^s = p^d, \quad (2.4)$$

$$\mathbf{u}^s \cdot \boldsymbol{\tau}_j = -2 \frac{\sqrt{\kappa_j}}{\alpha_1} D(\mathbf{u}^s) \mathbf{n}^s \cdot \boldsymbol{\tau}_j, \quad j = 1, \dots, N-1. \quad (2.5)$$

Here, Ω^i ($i = s, d$) denote bounded, simply connected polygonal or polyhedral in \mathbb{R}^N ($N = 2, 3$), and $\Gamma^i = \partial\Omega^i \setminus \Gamma$ are the boundaries. Unit normal vector \mathbf{n}^i are oriented outward from $\partial\Omega^i$, with $\mathbf{n}^s = -\mathbf{n}^d$ on Γ .

The solution pairs (\mathbf{u}^s, p^s) and (\mathbf{u}^d, p^d) satisfy Stokes and Darcy equations in their respective domains, where

- \mathbf{f}^i and g^i represent body forces and divergence constraints satisfying $\int_{\Omega^s} g^s + \int_{\Omega^d} g^d = 0$;
- μ denotes fluid viscosity;
- $D(\mathbf{u}^s) = (\nabla \mathbf{u}^s + (\nabla \mathbf{u}^s)^T)/2$ is the strain tensor;
- K is a symmetric positive definite permeability tensor satisfying

$$K_L \xi^T \xi \leq \xi^T K \xi \leq K_U \xi^T \xi, \quad \forall \xi \in \mathbb{R}^N,$$

for some constants $0 < K_L \leq K_U < \infty$;

- $\kappa_j = \boldsymbol{\tau}_j \cdot K \cdot \boldsymbol{\tau}_j$ with $\boldsymbol{\tau}_j$ being tangent vectors to Γ ;
- α_1 is an empirical Beavers-Joseph-Saffman (BJS) parameter.

The interface conditions enforce: (2.3) normal continuity, (2.4) balance of normal forces, and (2.5) the BJS slip condition.

Let $H^m(E)$ denote standard Sobolev spaces with norm $\|\cdot\|_{m,E}$ and seminorm $|\cdot|_{m,E}$ for subdomain $E \subset \mathbb{R}^N$. In particular, $H^0(E) = L^2(E)$ and the subscript m will be dropped from the norms. The norms are applicable to both vector valued functions in space $[H^m(E)]^N$ and tensor valued functions in space $[H^m(E)]^{N \times N}$ as well. Let $(\cdot, \cdot)_E$ denote the $L^2(E)$, $[L^2(E)]^N$, and $[L^2(E)]^{N \times N}$ inner product for scalar, vector, and tensor valued functions, respectively. In the above definition, if $E = \Omega^i$, $i = s, d$, we will abbreviate as $\|\cdot\|_{k,i}$, $|\cdot|_{k,i}$, and $(\cdot, \cdot)_i$. We also use $\langle \cdot, \cdot \rangle_\Gamma$ and $\|\cdot\|_\Gamma$ to denote the $L^2(\Gamma)$ inner product and norm, respectively, for scalar and vector valued functions.

We define:

$$L_0^2(E) = \{q \in L^2(E) \mid \int_E q = 0\},$$

$$H(\text{div}; E) = \{\mathbf{v} \in [L^2(E)]^N \mid \nabla \cdot \mathbf{v} \in L^2(E)\}.$$

The velocity spaces are:

$$\begin{aligned} V^s &= \{\mathbf{v}^s \in [H^1(\Omega^s)]^N \mid \mathbf{v}^s = \mathbf{0} \text{ on } \Gamma^s\}, \\ V^d &= \{\mathbf{v}^d \in H(\text{div}; \Omega^d) \mid \mathbf{v}^d \cdot \mathbf{n}^d = 0 \text{ on } \Gamma^d\}, \end{aligned}$$

equipped with the norm

$$\|\mathbf{v}\|_X = (|\mathbf{v}^s|_{1,s}^2 + \|\mathbf{v}^d\|_d^2 + \|\nabla \cdot \mathbf{v}^d\|_d^2)^{1/2}.$$

The composite velocity space incorporating interface condition (2.3) is:

$$V = \{\mathbf{v} = (\mathbf{v}^s, \mathbf{v}^d) \in V^s \times V^d \mid \langle \mathbf{v}^s \cdot \mathbf{n}^s + \mathbf{v}^d \cdot \mathbf{n}^d, \lambda \rangle_\Gamma = 0, \forall \lambda \in \Lambda\},$$

where $\Lambda = H_{00}^{1/2}(\Gamma) \subset L^2(\Gamma)$ follows the definition in [15]. The pressure space is $Q = L_0^2(\Omega)$ for $\Omega = \Omega^s \cup \Omega^d$.

The weak formulation of (2.1)-(2.5) reads: Find $(\mathbf{u}, p) \in V \times Q$ satisfying

$$a(\mathbf{u}, \mathbf{v}) + b(\mathbf{v}, p) = (\mathbf{f}, \mathbf{v}), \quad \forall \mathbf{v} \in V, \quad (2.6)$$

$$b(\mathbf{u}, q) = (g, q), \quad \forall q \in Q, \quad (2.7)$$

with bilinear forms

$$\begin{aligned} a(\mathbf{u}, \mathbf{v}) &= a_s(\mathbf{u}^s, \mathbf{v}^s) + a_d(\mathbf{u}^d, \mathbf{v}^d) + a_I(\mathbf{u}^s, \mathbf{v}^s) \\ &= 2\mu(D(\mathbf{u}^s), D(\mathbf{v}^s))_s + \mu(K^{-1}\mathbf{u}^d, \mathbf{v}^d)_d + \sum_{j=1}^{N-1} \frac{\alpha_1 \mu}{\sqrt{\kappa_j}} \langle \mathbf{u}^s \cdot \boldsymbol{\tau}_j, \mathbf{v}^s \cdot \boldsymbol{\tau}_j \rangle_\Gamma, \quad \forall \mathbf{u}, \mathbf{v} \in V^s \times V^d, \\ b(\mathbf{v}, q) &= -(\nabla \cdot \mathbf{v}^s, q)_s - (\nabla \cdot \mathbf{v}^d, q)_d, \quad \forall \mathbf{v} \in V^s \times V^d, q \in Q. \end{aligned}$$

The normal continuity condition (2.3) is enforced through the space V , while conditions (2.4) and (2.5) emerge naturally in the weak formulation. The well-posedness of this system is established in Theorem 3.1 of [15].

3 Classical FEM discretization

Let \mathcal{T}_h be a conforming and shape-regular triangulation, which consists of simplices and matches at Γ [15]. The set of edges or faces in \mathcal{T}_h is denoted by \mathcal{E}_h . Moreover, we define three useful sub-triangulation as following

$$\mathcal{E}_h(\Gamma) = \{e \in \mathcal{E}_h \mid e \subset \Gamma\}, \quad \mathcal{T}_h(\Omega^i) = \{T \in \mathcal{T}_h \mid T \subset \Omega^i\}, \quad i = s, d.$$

For $T \in \mathcal{T}_h$, let h_T denote the diameter of the polygon or polyhedra T and $h = \max_{T \in \mathcal{T}_h} h_T$. For the discretization of the fluid's variables in Ω^s , we choose finite element space $V_h^s \subset V^s$, $Q_h^s \subset L^2(\Omega^s)$ introduced in Section 4.1.1 in [19], which are LBB-stable. This velocity space is achieved by enriching the space $P_k(T)$, $k \geq 2$, of continuous, piece-wise polynomial functions of degree less than or equal to k with suitable bubble functions. The pressure space in Ω^s contains the functions with degree $k-1$ in Ω^s , i.e. $Q_h^s = \{q_h \in L^2(\Omega^s) \mid q_h|_T \in P_{k-1}(T), T \in \mathcal{T}_h(\Omega^s)\}$.

For any element $T \in \mathcal{T}_h$, let $\{z_0, \dots, z_d\}$ denote its vertices. We define barycentric coordinates $\lambda_j \in P_1(T)$, $0 \leq j \leq N$ uniquely such that $\lambda_j(z_l) = \delta_{jl}$, where δ_{jl} denotes the Kronecker delta function. Let b_T be the product of barycentric coordinates related to the element T , and let $\tilde{P}_l(T)$ denote the space of homogeneous polynomials of degree l . Indeed, we choose

$$V_h^s = \{\mathbf{v}_h^s \in V^s \mid \mathbf{v}_h^s|_T \in \mathbf{P}_k^+(T), T \in \mathcal{T}_h(\Omega^s)\} \quad \text{with} \quad \mathbf{P}_k^+(T) = [P_k(T) \oplus \text{span}\{b_T \tilde{P}_{k-2}(T)\}]^2,$$

in two-dimensional case and

$$V_h^s = \{\mathbf{v}_h^s \in V^s \mid \mathbf{v}_h^s|_T \in \mathbf{P}_k^+(T), T \in \mathcal{T}_h(\Omega^s)\},$$

for three-dimensional case with

$$\begin{aligned} \mathbf{P}_k^+(T) &= [P_k(T) \oplus \text{span}\{b_T(\tilde{P}_{k-2}(T) \oplus \tilde{P}_{k-3}(T))\}]^3, \quad k \geq 3, \\ \mathbf{P}_k^+(T) &= [P_k(T) \oplus b_T(\tilde{P}_{k-2}(T))]^3 \oplus \text{span}\{\mathbf{p}_1, \mathbf{p}_2, \mathbf{p}_3, \mathbf{p}_4\}, \quad k = 2 \end{aligned}$$

with the face bubble functions $\mathbf{p}_j = \mathbf{n}_j \prod_{l=1}^N \lambda_{j_l}$, where j_1, \dots, j_N are different indexes from the set $\{1, \dots, N+1\} \setminus \{j\}$ and \mathbf{n}_j is the outer normal of the face opposite the vertex $\lambda_j = 1$.

The porous medium problem in Ω^d , we choose mixed finite element spaces to be the RT_{k-1} spaces [23] for the normal velocity vanishing on boundary Γ^d , and the pressure space similar to fluid domain, denoted by V_h^d and Q_h^d . It is known for these choices that $V_h^d \subset V^d$, $Q_h^d \in L^2(\Omega^d)$, and $\nabla \cdot V_h^d = Q_h^d$.

On the interface Γ , define another finite element space, which is the normal trace of V_h^d on Γ_h , as following

$$\Lambda_h = \{\lambda_h \in L^2(\Gamma) \mid \mu_{h|e} \in [P_k(e)]^N, \forall e \in \mathcal{E}_h(\Gamma)\}.$$

With these spaces V_h^s, V_h^d , and Λ_h , define

$$V_h = \{\mathbf{v}_h = (\mathbf{v}_h^s, \mathbf{v}_h^d) \in V_h^s \times V_h^d \mid \langle \mathbf{v}_h^s \cdot \mathbf{n}^s + \mathbf{v}_h^d \cdot \mathbf{n}^d, \lambda_h \rangle_\Gamma = 0, \forall \lambda_h \in \Lambda_h\}. \quad (3.1)$$

Note that, since function $\lambda_h \in \Lambda_h$ does not in general vanish on $\partial\Gamma$ ($\Lambda_h \not\subset \Lambda$), the space V_h is nonconforming ($V_h \not\subset V$). With spaces Q_h^s and Q_h^d , define $Q_h = \{q \in Q_h^s \times Q_h^d \mid (q, 1)_\Omega = 0\}$, which is vanishing integral in Ω and satisfy $Q_h \subset Q$.

The classical variational discretization of (2.6)-(2.7) solves the following discrete problem: seek $(\mathbf{u}_h, p_h) \in V_h \times Q_h$ such that

$$\begin{aligned} a(\mathbf{u}_h, \boldsymbol{\psi}_h) + b(\boldsymbol{\psi}_h, p_h) &= (\mathbf{f}, \boldsymbol{\psi}_h), \quad \forall \boldsymbol{\psi}_h \in V_h, \\ b(\mathbf{u}_h, \phi_h) &= (g, \phi_h), \quad \forall \phi_h \in Q_h. \end{aligned} \quad (3.2)$$

The inf-sup condition of the pair $V_h^s \times Q_h^s$ can be get from Lemma 4.1 in [15] combining with the following Lemma 3.1. Then, the inf-sup conditions for the coupled problem holds form Lemma 4.3 in [15] which determines the solvability of the discrete problem. Although the pressure space Q_h^s is not restricted to have zero mean over Ω^s , i.e., $Q_h^s \subset L^2(\Omega^s)$, not $L_0^2(\Omega^s)$, the proof of Lemma 3.1 is similar to the usual one verified in the literature(VI.4 of [3]). To maintain the integrity of the text, we still provide the proof in Appendix A.

Remark 3.1. In this work, we use $\mathfrak{a} \lesssim \mathfrak{b}$ when there exists a constant c independent of $\mathfrak{a}, \mathfrak{b}, h, \mu$ such that $\mathfrak{a} \leq c\mathfrak{b}$.

Lemma 3.1. There exists an operator $\Upsilon_h^s : V^s \rightarrow V_1^s \subset V_h^s$ satisfying, for any $T \in \mathcal{T}_h(\Omega^s)$ and all $\mathbf{v}^s \in V^s$,

$$\int_T \nabla \cdot (\Upsilon_h^s \mathbf{v}^s - \mathbf{v}^s) = 0, \quad \text{and} \quad \|\Upsilon_h^s \mathbf{v}^s\|_s \lesssim \|\mathbf{v}^s\|_{1,s}, \quad (3.3)$$

where $V_1^s = \{\mathbf{v}_h^s \in V^s \mid \mathbf{v}_h^s|_T \in \mathbf{P}_1^+(T), T \in \mathcal{T}_h(\Omega^s)\}$ with $\mathbf{P}_1^+(T) = [P_1(T)]^N \oplus \text{span}\{\mathbf{p}_1, \dots, \mathbf{p}_{N+1}\}$.

Proof. The proof can be found in Appendix A. \square

Define

$$\begin{aligned} V(g) &= \{\boldsymbol{\psi} \in V \mid b(\boldsymbol{\psi}, \phi) = (g, \phi), \forall \phi \in Q\}, \\ V_h(g) &= \{\boldsymbol{\psi}_h \in V_h \mid b(\boldsymbol{\psi}_h, \phi_h) = (g, \phi_h), \forall \phi_h \in Q_h\}. \end{aligned}$$

for the inf-sup stable pair $V \times Q$ and $V_h \times Q_h$ with $V_h(g) \not\subset V(g)$ (since the divergence-free and normal continuity across Γ hold discretely).

The analysis is based on a pressure-related functional on V_h , which consists of relaxed divergence-free constraint and relaxed normal continuity across Γ . This functional is defined by

$$\vartheta_p(\boldsymbol{\psi}_h) = b(\boldsymbol{\psi}_h, p) - \langle \boldsymbol{\psi}_h^s \cdot \mathbf{n}^s + \boldsymbol{\psi}_h^d \cdot \mathbf{n}^d, p^d \rangle_\Gamma, \quad \forall \boldsymbol{\psi}_h \in V_h, \quad (3.4)$$

related to $p^d \in H^1(\Omega^d)$. For the function exactly satisfying divergence constraint and interface normal continuity, i.e. $\boldsymbol{\psi}_h \in V(0)$, or $p \in Q_h$ and $p^d \in \Lambda_h$, this functional is always zero. For the other cases, the functional $\vartheta_p(\boldsymbol{\psi}_h) \neq 0$, which leads to the discrete format being pressure-dependent. The following lemma is a direct corollary of the Lemma 3.1 in [17].

Lemma 3.2. *When $p^d \in H^1(\Omega^d)$, the functional defined in (3.4), is bounded and with the estimation*

$$\vartheta_p(\boldsymbol{\psi}_h) \lesssim \left(\inf_{\phi_h \in Q_h^s} \|p^s - \phi_h\|_s^2 + h \inf_{\phi_h \in \Lambda_h} \|p^d - \phi_h\|_\Gamma^2 \right)^{1/2} \|\boldsymbol{\psi}_h\|_X, \quad \forall \boldsymbol{\psi}_h \in V_h(0).$$

It is studied how the functional from the lack of pressure-robustness for the natural energy norm induced by the PDE. To do so, we estimate the distance of \mathbf{u}_h to the Stokes-Darcy best-approximation, denoted by $S_h \mathbf{u} \in V_h$, that is defined by

$$\begin{aligned} a(S_h \mathbf{u}, \boldsymbol{\psi}_h) + b(\boldsymbol{\psi}_h, \delta_h) &= a(\mathbf{u}, \boldsymbol{\psi}_h), \quad \forall \boldsymbol{\psi}_h \in V_h, \\ b(S_h \mathbf{u}, \phi_h) &= (g, \phi_h), \quad \forall \phi_h \in Q_h. \end{aligned} \quad (3.5)$$

Here δ_h denotes the pressure. Then for any $\mathbf{v}_h \in V_h$, from (3.5) and noting $(g, \phi_h) = b(\mathbf{u}, \phi_h)$, we have

$$\begin{aligned} a(S_h \mathbf{u} - \mathbf{v}_h, \boldsymbol{\psi}_h) + b(\boldsymbol{\psi}_h, \delta_h) &= a(\mathbf{u} - \mathbf{v}_h, \boldsymbol{\psi}_h), \quad \forall \boldsymbol{\psi}_h \in V_h, \\ b(S_h \mathbf{u} - \mathbf{v}_h, \phi_h) &= b(\mathbf{u} - \mathbf{v}_h, \phi_h), \quad \forall \phi_h \in Q_h. \end{aligned}$$

Since (V_h, Q_h) is LBB-stable shown in Lemma 4.3 in [15] combing Lemma 3.1, and operator $a(\cdot, \cdot)$ is coercive for $V^s \times \{\boldsymbol{\psi}^d \in V^d \mid \nabla \cdot \boldsymbol{\psi}^d = 0\}$ shown in Lemma 4.1 in [15], then the abstract bound estimates ([3], Chap II. Theorem 1.2) implies

$$\|S_h \mathbf{u} - \mathbf{v}_h\|_X \lesssim \|\mathbf{u} - \mathbf{v}_h\|_X,$$

which equals

$$\|\mathbf{u} - S_h \mathbf{u}\|_X \leq \inf_{\mathbf{v}_h \in V_h} (\|\mathbf{u} - \mathbf{v}_h\|_X + \|S_h \mathbf{u} - \mathbf{v}_h\|_X) \lesssim \inf_{\mathbf{v}_h \in V_h} \|\mathbf{u} - \mathbf{v}_h\|_X. \quad (3.6)$$

This shows convergence rates corresponding to the regularity of \mathbf{u} and the polynomial order of V_h . From the triangle inequality, this approximation result $\|\mathbf{u} - \mathbf{u}_h\|_X^2$ is only perturbed by the term $\|S_h \mathbf{u} - \mathbf{u}_h\|_X^2$ which therefore is the primal object of interest in the a priori error analysis below.

The error estimates involving the previously defined projector $S_h : V(g) \rightarrow V_h(g)$ in (3.5) needs to be discussed in the following theorem.

Theorem 3.1. *If the exact solutions of (2.6)-(2.7) have the regularity $\mathbf{u}^s \in [H^2(\Omega^s)]^N$, and $p^i \in H^1(\Omega^i)$, $i = s, d$, it holds*

$$\|S_h \mathbf{u} - \mathbf{u}_h\|_X^2 \lesssim \frac{1}{\mu^2} \left(\inf_{\phi_h \in Q_h^s} \|p^s - \phi_h\|_s^2 + h \inf_{\phi_h \in \Lambda_h} \|p^d - \phi_h\|_\Gamma^2 \right) + \|\mathbf{u} - S_h \mathbf{u}\|_X^2, \quad (3.7)$$

for the solution of \mathbf{u}_h of (3.2) and the discrete approximation $S_h \mathbf{u}$ of the exact solutions \mathbf{u} of (2.6)-(2.7). Furthermore, if the exact solutions of have the regularity $(\mathbf{u}^s, \mathbf{u}^d) \in [H^r(\Omega^s)]^N \times [H^{r-1}(\Omega^d)]^N$, $\nabla \cdot \mathbf{u}^d \in H^{r-1}(\Omega^d)$, and $p^i \in H^{r-1}(\Omega^i)$, $i = s, d$ for any $k \leq r \leq k+1$ with $k \geq 2$, it holds

$$\|\mathbf{u} - \mathbf{u}_h\|_X^2 \lesssim h^{2(r-1)} (\|\mathbf{u}^s\|_{r,s}^2 + \|\mathbf{u}^d\|_{r-1,d}^2 + \|\nabla \cdot \mathbf{u}^d\|_{r-1,d}^2 + \frac{1}{\mu^2} \|p^s\|_{r-1,s}^2 + \frac{1}{\mu^2} \|p^d\|_{r-1,d}^2), \quad (3.8)$$

and

$$\|p - p_h\|^2 \lesssim h^{2(r-1)} (\mu^2 \|\mathbf{u}^s\|_{r,s}^2 + \mu^2 \|\mathbf{u}^d\|_{r-1,d}^2 + \mu^2 \|\nabla \cdot \mathbf{u}^d\|_{r-1,d}^2 + \|p^s\|_{r-1,s}^2 + \|p^d\|_{r-1,d}^2). \quad (3.9)$$

Proof. For any $\boldsymbol{\psi}_h \in V_h$, according to the definition of $a(\cdot, \cdot)$ in (2.6), we have

$$a(\mathbf{u}, \boldsymbol{\psi}_h) = 2\mu(D(\mathbf{u}^s), D(\boldsymbol{\psi}_h^s))_s + \mu(K^{-1}\mathbf{u}^d, \boldsymbol{\psi}_h^d)_d + \sum_{j=1}^{N-1} \frac{\alpha_1\mu}{\sqrt{\kappa_j}} \langle \mathbf{u}^s \cdot \boldsymbol{\tau}_j, \boldsymbol{\psi}_h^s \cdot \boldsymbol{\tau}_j \rangle_\Gamma. \quad (3.10)$$

Since $\mathbf{u}^s \in [H^2(\Omega^s)]^N$ and $p^i \in H^1(\Omega^i)$, $i = s, d$, the solutions (\mathbf{u}, p) of (2.6)~(2.7) satisfy (2.1)~(2.5). Then, based on the usual integration by parts and the boundary condition (2.5), the first and the third summands in (3.10) can be derived into

$$2\mu(D(\mathbf{u}^s), D(\boldsymbol{\psi}_h^s))_s = -2\mu(\nabla \cdot D(\mathbf{u}^s), \boldsymbol{\psi}_h^s)_s + 2\mu\langle D(\mathbf{u}^s)\mathbf{n}^s, \boldsymbol{\psi}_h^s \rangle_\Gamma, \quad (3.11)$$

$$\sum_{j=1}^{N-1} \frac{\alpha_1\mu}{\sqrt{\kappa_j}} \langle \mathbf{u}^s \cdot \boldsymbol{\tau}_j, \boldsymbol{\psi}_h^s \cdot \boldsymbol{\tau}_j \rangle_\Gamma = \sum_{j=1}^{N-1} -2\mu\langle D(\mathbf{u}^s)\mathbf{n}^s \cdot \boldsymbol{\tau}_j, \boldsymbol{\psi}_h^s \cdot \boldsymbol{\tau}_j \rangle_\Gamma. \quad (3.12)$$

From (3.10), (3.11), (3.12), and noting the Stokes-Darcy equations in (2.1) and (2.2), and basing on the equality

$$2\mu\langle D(\mathbf{u}^s)\mathbf{n}^s, \boldsymbol{\psi}_h^s \rangle_\Gamma = \sum_{j=1}^{N-1} 2\mu\langle D(\mathbf{u}^s)\mathbf{n}^s \cdot \boldsymbol{\tau}_j, \boldsymbol{\psi}_h^s \cdot \boldsymbol{\tau}_j \rangle_\Gamma + 2\mu\langle D(\mathbf{u}^s)\mathbf{n}^s \cdot \mathbf{n}^s, \boldsymbol{\psi}_h^s \cdot \mathbf{n}^s \rangle_\Gamma, \quad (3.13)$$

we have

$$a(\mathbf{u}, \boldsymbol{\psi}_h) = (\mathbf{f}, \boldsymbol{\psi}_h) - (\nabla p^s, \boldsymbol{\psi}_h^s)_s - (\nabla p^d, \boldsymbol{\psi}_h^d)_d + 2\mu\langle D(\mathbf{u}^s)\mathbf{n}^s \cdot \mathbf{n}^s, \boldsymbol{\psi}_h^s \cdot \mathbf{n}^s \rangle_\Gamma.$$

By using the integration by parts for the second and third terms in the above equation, and nothing the boundary condition in (2.4), it can be obtained that

$$\begin{aligned} -(\nabla p^s, \boldsymbol{\psi}_h^s)_s - (\nabla p^d, \boldsymbol{\psi}_h^d)_d &= (p^s, \nabla \cdot \boldsymbol{\psi}_h^s)_s - \langle p^s, \boldsymbol{\psi}_h^s \cdot \mathbf{n}^s \rangle_\Gamma + (p^d, \nabla \cdot \boldsymbol{\psi}_h^d)_d - \langle p^d, \boldsymbol{\psi}_h^d \cdot \mathbf{n}^d \rangle_\Gamma \\ &= -b(\boldsymbol{\psi}_h, p) - 2\mu\langle D(\mathbf{u}^s)\mathbf{n}^s \cdot \mathbf{n}^s, \boldsymbol{\psi}_h^s \cdot \mathbf{n}^s \rangle_\Gamma - \langle p^d, \boldsymbol{\psi}_h^s \cdot \mathbf{n}^s + \boldsymbol{\psi}_h^d \cdot \mathbf{n}^d \rangle_\Gamma \end{aligned}$$

Thus, combining with (3.4), we have

$$\begin{aligned} a(\mathbf{u}, \boldsymbol{\psi}_h) &= (\mathbf{f}, \boldsymbol{\psi}_h) - b(\boldsymbol{\psi}_h, p) - \langle p^d, \boldsymbol{\psi}_h^s \cdot \mathbf{n}^s + \boldsymbol{\psi}_h^d \cdot \mathbf{n}^d \rangle_\Gamma \\ &= (\mathbf{f}, \boldsymbol{\psi}_h) - \vartheta_p(\boldsymbol{\psi}_h). \end{aligned} \quad (3.14)$$

From (3.5), it is clear that $S_h\mathbf{u} \in V_h(g)$. Since $S_h\mathbf{u} - \mathbf{u}_h \in V_h(0)$ and $\nabla \cdot V_h^d = Q_h^d$, it can be obtained $\nabla \cdot (S_h\mathbf{u} - \mathbf{u}_h)^d = 0$. Then, from Lemma 3.1 in [15], (3.5), (3.14), and the boundness of $a(\cdot, \cdot)$ and ϑ_p , it reveals

$$\begin{aligned} \mu\|S_h\mathbf{u} - \mathbf{u}_h\|_X^2 &\lesssim a(S_h\mathbf{u} - \mathbf{u}_h, S_h\mathbf{u} - \mathbf{u}_h) \\ &= a(S_h\mathbf{u} - \mathbf{u}, S_h\mathbf{u} - \mathbf{u}_h) + a(\mathbf{u} - \mathbf{u}_h, S_h\mathbf{u} - \mathbf{u}_h) \\ &= a(S_h\mathbf{u} - \mathbf{u}, S_h\mathbf{u} - \mathbf{u}_h) + (\mathbf{f}, S_h\mathbf{u} - \mathbf{u}_h) - \vartheta_p(S_h\mathbf{u} - \mathbf{u}_h) \\ &\quad - (\mathbf{f}, S_h\mathbf{u} - \mathbf{u}_h) \\ &= a(S_h\mathbf{u} - \mathbf{u}, S_h\mathbf{u} - \mathbf{u}_h) - \vartheta_p(S_h\mathbf{u} - \mathbf{u}_h) \\ &\lesssim \mu\|S_h\mathbf{u} - \mathbf{u}\|_X\|S_h\mathbf{u} - \mathbf{u}_h\|_X + \vartheta_p(S_h\mathbf{u} - \mathbf{u}_h), \end{aligned}$$

which implies (3.7).

Next, we will prove (3.8). If $p^i \in H^{r-1}(\Omega^i)$, $i = s, d$ for any $k \leq r \leq k+1$ with $k \geq 2$, let ϕ_h^d to be the local L^2 projection of p^d into $\{q_h \in L^2(\Omega^d) \mid q_h|_T \in P_{k-1}(T), T \in \mathcal{T}_h(\Omega^d)\}$. From

Lemma 3.2, projection property, and trace inequality, we have

$$\begin{aligned}
& \inf_{\phi_h \in Q_h^s} \|p^s - \phi_h\|_s^2 + h \inf_{\phi_h \in \Lambda_h} \|p^d - \phi_h\|_\Gamma^2 \\
& \lesssim h^{2(r-1)} \|p^s\|_{r-1,s}^2 + h \|p^d - \phi_h^d\|_\Gamma^2 \\
& \lesssim h^{2(r-1)} \|p^s\|_{r-1,s}^2 + h \sum_{T \in \mathcal{T}_h(\Gamma^d)} h_T^{-1} \|p^d - \phi_h^d\|_T^2 + h_T \|\nabla(p^d - \phi_h^d)\|_T^2 \\
& \lesssim h^{2(r-1)} \|p^s\|_{r-1,s}^2 + h \sum_{T \in \mathcal{T}_h(\Gamma^d)} h_T^{2(r-1)-1} \|p^d\|_{r-1,T}^2 \\
& \lesssim h^{2(r-1)} (\|p^s\|_{r-1,s}^2 + \|p^d\|_{r-1,d}^2),
\end{aligned} \tag{3.15}$$

where $\mathcal{T}_h(\Gamma^d) = \{T \in \mathcal{T}_h(\Omega^d) \mid T \cap \Gamma \neq \emptyset\}$.

For the terms $\|\mathbf{u} - S_h \mathbf{u}\|_X^2$ in (3.7), if $(\mathbf{u}^s, \mathbf{u}^d) \in [H^r(\Omega^s)]^N \times [H^{r-1}(\Omega^d)]^N$ and $\nabla \cdot \mathbf{u}^d \in H^{r-1}(\Omega^d)$ for any $k \leq r \leq k+1$ with $k \geq 2$, from the approximation property (3.6) and the interpolation properties introduced in [15] (in which, refer to (4.3), (4.13), (4.14), and (4.35)), it is obtained

$$\begin{aligned}
\|\mathbf{u} - S_h \mathbf{u}\|_X^2 & \lesssim \inf_{\mathbf{v}_h \in V_h} \|\mathbf{u} - \mathbf{v}_h\|_X^2 \\
& = \inf_{\mathbf{v}_h \in V_h} |\mathbf{u}^s - \mathbf{v}_h^s|_{1,s}^2 + \|\mathbf{u}^d - \mathbf{v}_h^d\|_d^2 + \|\nabla \cdot (\mathbf{u}^d - \mathbf{v}_h^d)\|_d^2 \\
& \lesssim h^{2(r-1)} (\|\mathbf{u}^s\|_{r,s}^2 + \|\mathbf{u}^d\|_{r-1,d}^2 + \|\nabla \cdot \mathbf{u}^d\|_{r-1,d}^2).
\end{aligned} \tag{3.16}$$

Combining with (3.15) and (3.16), it yields (3.8).

Finally, we show the proof of (3.9) with the regularity $(\mathbf{u}^s, \mathbf{u}^d) \in [H^r(\Omega^s)]^N \times [H^{r-1}(\Omega^d)]^N$, $\nabla \cdot \mathbf{u}^d \in H^{r-1}(\Omega^d)$, and $p^i \in H^{r-1}(\Omega^i)$, $i = s, d$ for any $k \leq r \leq k+1$ with $k \geq 2$. Let $P_h p$ to be the local L^2 projection of p into Q_h . From (3.14), we can get

$$\begin{aligned}
b(\psi_h, P_h p - p_h) & = b(\psi_h, P_h p) + a(\mathbf{u}_h, \psi_h) - (\mathbf{f}, \psi_h) \\
& = a(\mathbf{u}, \psi_h) + b(\psi_h, P_h p) - (\mathbf{f}, \psi_h) - a(\mathbf{u} - \mathbf{u}_h, \psi_h) \\
& = b(\psi_h, P_h p - p) - \langle p^d, \psi_h^s \cdot \mathbf{n}^s + \psi_h^d \cdot \mathbf{n}^d \rangle_\Gamma - a(\mathbf{u} - \mathbf{u}_h, \psi_h).
\end{aligned} \tag{3.17}$$

Then, we give the boundedness of $\langle p^d, \psi_h^s \cdot \mathbf{n}^s + \psi_h^d \cdot \mathbf{n}^d \rangle_\Gamma$ in (3.17). To begin with, let $\lambda_h \in \Lambda_h$ to be the local L^2 projection of $p|_\Gamma$ into Λ_h , i.e. $\langle p^d - \lambda_h, \phi_h \rangle_e = 0$ for any $\phi_h \in P_{k-1}(e)$, $e \in \mathcal{E}_h(\Gamma)$.

Noting the fact $\psi_h^d \cdot \mathbf{n}_\Gamma^d \in \Lambda_h$, it holds

$$\langle \psi_h^d \cdot \mathbf{n}^d, p^d - \lambda_h \rangle_\Gamma = 0. \tag{3.18}$$

Let $\bar{\psi}_h^s$ to be the local L^2 projection of ψ_h^s into $\{\mathbf{v}_h \in [L^2(\Omega^s)]^N \mid \mathbf{v}_h|_T \in [P_{k-1}(T)]^N, T \in \mathcal{T}_h(\Omega^s)\}$. From $\bar{\psi}_h^s \cdot \mathbf{n}_\Gamma^s \in \Lambda_h$, Cauchy-Schwarz inequality, trace inequality, and projection property, we have

$$\begin{aligned}
& \langle \psi_h^s \cdot \mathbf{n}^s, p^d - \lambda_h \rangle_\Gamma \\
& = \langle \psi_h^s \cdot \mathbf{n}^s - \bar{\psi}_h^s \cdot \mathbf{n}^s, p^d - \lambda_h \rangle_\Gamma \\
& \leq \|\psi_h^s \cdot \mathbf{n}^s - \bar{\psi}_h^s \cdot \mathbf{n}^s\|_\Gamma \inf_{\phi_h \in \Lambda_h} \|p^d - \phi_h\|_\Gamma \\
& \leq \left(\sum_{T \in \mathcal{T}_h(\Gamma^s)} h_T^{-1} \|\psi_h^s - \bar{\psi}_h^s\|_{0,T}^2 + h_T |\psi_h^s - \bar{\psi}_h^s|_{1,T}^2 \right)^{1/2} \inf_{\phi_h \in \Lambda_h} \|p^d - \phi_h\|_\Gamma \\
& \leq \left(\sum_{T \in \mathcal{T}_h(\Gamma^s)} h_T |\psi_h^s|_{1,T}^2 \right)^{1/2} \inf_{\phi_h \in \Lambda_h} \|p^d - \phi_h\|_\Gamma,
\end{aligned} \tag{3.19}$$

where $\mathcal{T}_h(\Gamma^s) = \{T \in \mathcal{T}_h(\Omega^s) \mid T \cap \Gamma \neq \emptyset\}$. From (3.18), (3.19), and $\langle \lambda_h, \boldsymbol{\psi}_h^s \cdot \mathbf{n}^s + \boldsymbol{\psi}_h^d \cdot \mathbf{n}^d \rangle_\Gamma = 0$, it can be obtained

$$\langle p^d, \boldsymbol{\psi}_h^s \cdot \mathbf{n}^s + \boldsymbol{\psi}_h^d \cdot \mathbf{n}^d \rangle_\Gamma \lesssim \left(\sum_{T \in \mathcal{T}_h(\Gamma^s)} h_T |\boldsymbol{\psi}_h^s|_{1,T}^2 \right)^{1/2} \inf_{\phi_h \in \Lambda_h} \|p^d - \phi_h\|_\Gamma. \quad (3.20)$$

Combining the boundedness of operators $a(\cdot, \cdot)$ and $b(\cdot, \cdot)$, (3.17), and (3.20), we conclude that

$$b(\boldsymbol{\psi}_h, P_h p - p_h) \lesssim (\|P_h p - p\| + h^{1/2} \inf_{\phi_h \in \Lambda_h} \|p^d - \phi_h\|_\Gamma + \mu \|\mathbf{u} - \mathbf{u}_h\|_X) \|\boldsymbol{\psi}\|_X,$$

and

$$\begin{aligned} \|P_h p - p_h\| &\lesssim \sup_{\boldsymbol{\psi}_h \in V_h} \frac{b(\boldsymbol{\psi}_h, P_h p - p_h)}{\|\boldsymbol{\psi}_h\|_X} \\ &\lesssim \|P_h p - p\| + h^{1/2} \inf_{\phi_h \in \Lambda_h} \|p^d - \phi_h\|_\Gamma + \mu \|\mathbf{u} - \mathbf{u}_h\|_X. \end{aligned} \quad (3.21)$$

From the triangle inequality, (3.21), the projection property for $\|P_h p - p\|$, a discussion similar to (3.15) for $h^{1/2} \inf_{\phi_h \in \Lambda_h} \|p^d - \phi_h\|_\Gamma$, and (3.8), we get (3.9) and complete the proof. \square

Remark 3.2. *The pressure dependency come from the presence of a function in $V_h(0)$, which either does not satisfy exactly divergence-free or does not satisfy interface normal continuity.*

4 Pressure-robust discretization

In this section, we will apply a reconstruction operator to the discretization scheme to achieve exactly divergence-free and interface normal continuity, thereby obtaining a pressure-robust discretization. Therefore, for any $T \in \mathcal{T}_h$, we consider the Raviart-Thomas space $RT_{k-1}(T) = [P_{k-1}(T)]^N + \mathbf{x}P_{k-1}(T)$ for $k \geq 2$. We get for $\mathbf{v}_h \in RT_{k-1}(T)$ that $\nabla \cdot \mathbf{v}_h \in P_{k-1}(T)$, $\mathbf{v}_h \cdot \mathbf{n}|_e \in P_{k-1}(e)$, $e \subset \partial T$. Then, define

$$\Theta_h^i = \{\mathbf{v}_h \in H(\text{div}; \Omega^i) \mid \mathbf{v}_h|_T \in RT_{k-1}(T), \forall T \in \mathcal{T}_h, \mathbf{v}_h \cdot \mathbf{n} = 0 \text{ on } \Gamma^i\},$$

with $i = s, d$, respectively. Note that $\Theta_h^d = V_h^d$. Then, we define reconstruction operators $\Pi_h^i : V^i \rightarrow \Theta_h^i$ locally by

$$(\Pi_h^i \mathbf{v} - \mathbf{v}, \boldsymbol{\psi}_h)_T = 0, \quad \boldsymbol{\psi}_h \in [P_{k-2}(T)]^N, \quad (4.1)$$

$$\langle (\Pi_h^i \mathbf{v} - \mathbf{v}) \cdot \mathbf{n}, q_h \rangle_e = 0, \quad q_h \in P_{k-1}(e), e \subset \partial T, \quad (4.2)$$

for any element $T \subset \Omega^i$. From (2.5.10) and Proposition 2.5.1 in [2], the reconstruction operators are well defined with the property

$$\|\mathbf{v} - \Pi_h^i \mathbf{v}\|_{\ell, T} \lesssim h_T^{m-\ell} |\mathbf{v}|_{m, T}, \quad \ell = 0, 1, \quad (4.3)$$

for any $\mathbf{v} \in H^m(\Omega^i)$ and $1 \leq m \leq k$.

Next, we rewrite the Lemma 4.1 in [17] into a more detailed conclusion. The proof is the same as the original one. To maintain the integrity of the text, we still provide the proof in Appendix B.

Lemma 4.1. *Define $\Pi_h = \Pi_h^s \times \Pi_h^d : V^s \times V^d \rightarrow \Theta_h = \Theta_h^s \times \Theta_h^d$, which has the following properties*

$$\Pi_h : V_h \rightarrow \Theta_h \cap \Theta_b, \quad (4.4)$$

$$\Pi_h : V_h(0) \rightarrow \Theta_h \cap \Theta_d \cap \Theta_b. \quad (4.5)$$

where

$$\Theta_b = \{\boldsymbol{\psi} \in H(\text{div}, \Omega) \mid (\boldsymbol{\psi}_s \cdot \mathbf{n}^s)|_{\Gamma^s} = 0, (\boldsymbol{\psi}_d \cdot \mathbf{n}^d)|_{\Gamma^d} = 0, \text{ and } (\boldsymbol{\psi}^s \cdot \mathbf{n}^s + \boldsymbol{\psi}^d \cdot \mathbf{n}^d)|_\Gamma = 0\},$$

$$\Theta_d = \{\boldsymbol{\psi} \in H(\text{div}, \Omega) \mid \nabla \cdot \boldsymbol{\psi} = 0\}.$$

Proof. The proof can be found in Appendix B. \square

Lemma 4.2. For any $\boldsymbol{\psi}_h^s \in V_h^s$ and $\mathbf{u}^s \in [H^2(\Omega^s)]^N$, we have the following estimates

$$2\mu\langle \nabla \cdot D(\mathbf{u}^s), (1 - \Pi_h^s)\boldsymbol{\psi}_h^s \rangle_s \lesssim \mu \left(h^2 \sum_{T \in \mathcal{T}_h(\Omega^s)} \inf_{\boldsymbol{\varphi}_h^s \in [P_{k-2}(T)]^N} \|\nabla \cdot D(\mathbf{u}^s) - \boldsymbol{\varphi}_h^s\|_T^2 \right)^{1/2} \|\nabla \boldsymbol{\psi}_h^s\|_s,$$

$$2\mu\langle D(\mathbf{u}^s)\mathbf{n}^s \cdot \mathbf{n}^s, (1 - \Pi_h^s)\boldsymbol{\psi}_h^s \cdot \mathbf{n}^s \rangle_\Gamma \lesssim \mu \left(h \sum_{e \in \mathcal{E}_h(\Gamma)} \inf_{q_h \in P_{k-1}(e)} \|D(\mathbf{u}^s)\mathbf{n}^s \cdot \mathbf{n}^s - q_h\|_e^2 \right)^{1/2} \|\nabla \boldsymbol{\psi}_h^s\|_s.$$

Proof. For the first term, it is a direct conclusion from the orthogonality property (4.1), Cauchy-Schwarz inequality, estimation (4.3).

For the second estimate, from the orthogonality property (4.2) and Cauchy-Schwarz inequality, we have

$$\begin{aligned} & 2\mu\langle D(\mathbf{u}^s)\mathbf{n}^s \cdot \mathbf{n}^s, (1 - \Pi_h^s)\boldsymbol{\psi}_h^s \cdot \mathbf{n}^s \rangle_\Gamma \\ & \lesssim \mu \sum_{e \in \mathcal{E}_h(\Gamma)} \inf_{q_h \in P_{k-1}(e)} \|D(\mathbf{u}^s)\mathbf{n}^s \cdot \mathbf{n}^s - q_h\|_e \|(1 - \Pi_h^s)\boldsymbol{\psi}_h^s \cdot \mathbf{n}^s\|_e \\ & \lesssim \mu \left(\sum_{e \in \mathcal{E}_h(\Gamma)} \inf_{q_h \in P_{k-1}(e)} \|D(\mathbf{u}^s)\mathbf{n}^s \cdot \mathbf{n}^s - q_h\|_e^2 \right)^{1/2} \left(\sum_{e \in \mathcal{E}_h(\Gamma)} \|(1 - \Pi_h^s)\boldsymbol{\psi}_h^s \cdot \mathbf{n}^s\|_e^2 \right)^{1/2}. \end{aligned}$$

Using trace inequality and estimation (4.3), it can be obtained

$$\begin{aligned} & \sum_{e \in \mathcal{E}_h(\Gamma)} \|(1 - \Pi_h^s)\boldsymbol{\psi}_h^s \cdot \mathbf{n}^s\|_e^2 \\ & \lesssim \sum_{T \in \mathcal{T}_h(\Gamma^s)} h_T^{-1} \|(1 - \Pi_h^s)\boldsymbol{\psi}_h^s\|_T^2 + h_T \|\nabla(1 - \Pi_h^s)\boldsymbol{\psi}_h^s\|_T^2 \\ & \lesssim h \|\nabla \boldsymbol{\psi}_h^s\|_s^2, \end{aligned} \tag{4.6}$$

where $\mathcal{T}_h(\Gamma^s)$ is defined in (3.19). The above two inequalities imply the second estimate and we complete the proof. \square

To obtain a fully pressure-robust discretization, the Stokes-Darcy equations needs to be modified as follows: Find $(\mathbf{u}_h, p_h) \in V_h \times Q_h$ solving

$$\begin{aligned} a(\mathbf{u}_h, \boldsymbol{\psi}_h) + b(\boldsymbol{\psi}_h, p_h) &= (f, \Pi_h \boldsymbol{\psi}_h), \quad \forall \boldsymbol{\psi}_h \in V_h, \\ b(\boldsymbol{\psi}_h, \phi_h) &= (g, \phi_h), \quad \forall \phi_h \in Q_h. \end{aligned} \tag{4.7}$$

The analysis is based on an improved pressure-related functional with reconstruction operator on V_h , which achieves exact divergence-free and continuity across Γ . This functional is defined by

$$\mathfrak{N}_p(\boldsymbol{\psi}_h) = b(\Pi_h \boldsymbol{\psi}_h, p) - \langle \Pi_h^s \boldsymbol{\psi}_h^s \cdot \mathbf{n}^s + \Pi_h^d \boldsymbol{\psi}_h^d \cdot \mathbf{n}^d, p^d \rangle_\Gamma, \quad \forall \boldsymbol{\psi}_h \in V_h, \tag{4.8}$$

related to $p^d \in H^1(\Omega^d)$. Lemma 4.1 implies $\mathfrak{N}_p(\boldsymbol{\psi}_h) = 0$ for any $\boldsymbol{\psi}_h \in V_h(0)$ and any $p \in Q$ with $p^d \in H^1(\Omega^d)$, which leads to the discrete format being pressure-independent.

Theorem 4.1. If the exact solutions of (2.6) and (2.7) have the regularity $\mathbf{u}^s \in [H^2(\Omega^s)]^N$, and $p^i \in H^1(\Omega^i)$, $i = s, d$, it holds

$$\begin{aligned} \|S_h \mathbf{u} - \mathbf{u}_h\|_X^2 & \lesssim h^2 \sum_{T \in \mathcal{T}_h(\Omega^s)} \inf_{\boldsymbol{\varphi}_h^s \in [P_{k-2}(T)]^N} \|\nabla \cdot D(\mathbf{u}^s) - \boldsymbol{\varphi}_h^s\|_T^2 \\ & + h \sum_{e \in \mathcal{E}_h(\Gamma)} \inf_{q_h \in P_{k-1}(e)} \|D(\mathbf{u}^s)\mathbf{n}^s \cdot \mathbf{n}^s - q_h\|_e^2, \end{aligned} \tag{4.9}$$

for the solution \mathbf{u}_h of (4.7) and the discrete approximation $S_h \mathbf{u}$ of the exact solutions of (2.6) and (2.7). Furthermore, if the exact solutions have the regularity $(\mathbf{u}^s, \mathbf{u}^d) \in [H^r(\Omega^s)]^N \times [H^{r-1}(\Omega^d)]^N$, $\nabla \cdot \mathbf{u}^d \in H^{r-1}(\Omega^d)$, and $p^i \in H^{r-1}(\Omega^i)$, $i = s, d$ for any $k \leq r \leq k+1$ with $k \geq 2$, it holds

$$\|\mathbf{u} - \mathbf{u}_h\|_X^2 \lesssim h^{2(r-1)} (\|\mathbf{u}^s\|_{r,s}^2 + \|\mathbf{u}^d\|_{r-1,d}^2 + \|\nabla \cdot \mathbf{u}^d\|_{r-1,d}^2), \quad (4.10)$$

and

$$\|p - p_h\|^2 \lesssim h^{2(r-1)} (\mu^2 \|\mathbf{u}^s\|_{r,s}^2 + \mu^2 \|\mathbf{u}^d\|_{r-1,d}^2 + \mu^2 \|\nabla \cdot \mathbf{u}^d\|_{r-1,d}^2 + \|p^s\|_{r-1,s}^2 + \|p^d\|_{r-1,d}^2). \quad (4.11)$$

Proof. Since $\mathbf{u}^s \in [H^2(\Omega^s)]^N$ and $p^i \in H^1(\Omega^i)$, $i = s, d$, the solutions (\mathbf{u}, p) of (2.6) and (2.7) satisfy (2.1)~(2.5). From the property of the projector S_h in (3.5), the integration by parts, (2.1), (2.2), the boundary condition (2.5), it reveals

$$\begin{aligned} & \mu \|S_h \mathbf{u} - \mathbf{u}_h\|_X^2 \\ & \lesssim a(\mathbf{u} - \mathbf{u}_h, S_h \mathbf{u} - \mathbf{u}_h) \\ & = -2\mu \langle \nabla \cdot D(\mathbf{u}^s), (S_h \mathbf{u} - \mathbf{u}_h)^s \rangle_s + \mu \langle K^{-1} \mathbf{u}^d, (S_h \mathbf{u} - \mathbf{u}_h)^d \rangle_d \\ & \quad + 2\mu \langle D(\mathbf{u}^s) \mathbf{n}^s \cdot \mathbf{n}^s, (S_h \mathbf{u} - \mathbf{u}_h)^s \cdot \mathbf{n}^s \rangle_\Gamma - \langle \mathbf{f}, \Pi_h(S_h \mathbf{u} - \mathbf{u}_h) \rangle \\ & = -2\mu \langle \nabla \cdot D(\mathbf{u}^s), (1 - \Pi_h^s)(S_h \mathbf{u} - \mathbf{u}_h)^s \rangle_s + \mu \langle K^{-1} \mathbf{u}^d, (1 - \Pi_h^d)(S_h \mathbf{u} - \mathbf{u}_h)^d \rangle_d \\ & \quad + 2\mu \langle D(\mathbf{u}^s) \mathbf{n}^s \cdot \mathbf{n}^s, (S_h \mathbf{u} - \mathbf{u}_h)^s \cdot \mathbf{n}^s \rangle_\Gamma \\ & \quad - \langle \nabla p^s, \Pi_h^s(S_h \mathbf{u} - \mathbf{u}_h)^s \rangle_s - \langle \nabla p^d, \Pi_h^d(S_h \mathbf{u} - \mathbf{u}_h)^d \rangle_d. \end{aligned}$$

For the last two terms, using the integration by parts, the boundary condition (2.4), and Lemma 4.1 (implying the pressure-related term $\mathfrak{N}_p(S_h \mathbf{u} - \mathbf{u}_h) = 0$), we have

$$\begin{aligned} & - \langle \nabla p^s, \Pi_h^s(S_h \mathbf{u} - \mathbf{u}_h)^s \rangle_s - \langle \nabla p^d, \Pi_h^d(S_h \mathbf{u} - \mathbf{u}_h)^d \rangle_d \\ & = -b(\Pi_h(S_h \mathbf{u} - \mathbf{u}_h), p) - \langle p^s, \Pi_h^s(S_h \mathbf{u} - \mathbf{u}_h)^s \cdot \mathbf{n}^s \rangle_\Gamma - \langle p^d, \Pi_h^d(S_h \mathbf{u} - \mathbf{u}_h)^d \cdot \mathbf{n}^d \rangle_\Gamma \\ & = -b(\Pi_h(S_h \mathbf{u} - \mathbf{u}_h), p) - \langle p^d, \Pi_h^s(S_h \mathbf{u} - \mathbf{u}_h)^s \cdot \mathbf{n}^s \rangle_\Gamma + \langle p^d, \Pi_h^d(S_h \mathbf{u} - \mathbf{u}_h)^d \cdot \mathbf{n}^d \rangle_\Gamma \\ & \quad - 2\mu \langle D(\mathbf{u}^s) \mathbf{n}^s \cdot \mathbf{n}^s, \Pi_h^s(S_h \mathbf{u} - \mathbf{u}_h)^s \cdot \mathbf{n}^s \rangle_\Gamma \\ & = -\mathfrak{N}_p(S_h \mathbf{u} - \mathbf{u}_h) - 2\mu \langle D(\mathbf{u}^s) \mathbf{n}^s \cdot \mathbf{n}^s, \Pi_h^s(S_h \mathbf{u} - \mathbf{u}_h)^s \cdot \mathbf{n}^s \rangle_\Gamma \\ & = -2\mu \langle D(\mathbf{u}^s) \mathbf{n}^s \cdot \mathbf{n}^s, \Pi_h^s(S_h \mathbf{u} - \mathbf{u}_h)^s \cdot \mathbf{n}^s \rangle_\Gamma. \end{aligned}$$

Combining the above equations and noting $(1 - \Pi_h^d)(S_h \mathbf{u} - \mathbf{u}_h)^d = 0$, we have

$$\begin{aligned} \mu \|S_h \mathbf{u} - \mathbf{u}_h\|_X^2 & \lesssim ((-2\mu \nabla \cdot D(\mathbf{u}^s)), (1 - \Pi_h)(S_h \mathbf{u} - \mathbf{u}_h)) \\ & \quad + 2\mu \langle D(\mathbf{u}^s) \mathbf{n}^s \cdot \mathbf{n}^s, (1 - \Pi_h^s)(S_h \mathbf{u} - \mathbf{u}_h)^s \cdot \mathbf{n}^s \rangle_\Gamma. \end{aligned} \quad (4.12)$$

Then, Lemma 4.2 and (4.12) imply (4.9).

Next, we will prove (4.10) under the regularity $(\mathbf{u}^s, \mathbf{u}^d) \in [H^r(\Omega^s)]^N \times [H^{r-1}(\Omega^d)]^N$ and $\nabla \cdot \mathbf{u}^d \in H^{r-1}(\Omega^d)$ for any $k \leq r \leq k+1$ with $k \geq 2$. For the first term in (4.9), from Lemma 4.2 and projection property, we have

$$h^2 \sum_{T \in \mathcal{T}_h(\Omega^s)} \inf_{\varphi_h^s \in [P_{k-2}(T)]^N} \|\nabla \cdot D(\mathbf{u}^s) - \varphi_h^s\|_T^2 \lesssim h^{2(r-1)} \|\mathbf{u}^s\|_{r,s}^2. \quad (4.13)$$

For the second term in (4.9), let Ψ_h^s to be the local L^2 projection of $D(\mathbf{u}^s)$ into $\{\Phi_h \in [L^2(\Omega^s)]^{N \times N} \mid \Phi_h|_T \in [P_{k-1}(T)]^{N \times N}, T \in \mathcal{T}_h(\Omega^s)\}$. From Lemma 4.2, trace inequality, and

projection property, it is obtained

$$\begin{aligned}
& h \sum_{e \in \mathcal{E}_h(\Gamma)} \inf_{q_h \in P_{k-1}(e)} \|D(\mathbf{u}^s) \mathbf{n}^s \cdot \mathbf{n}^s - q_h\|_e^2 \\
& \lesssim h \sum_{e \in \mathcal{E}_h(\Gamma)} \|D(\mathbf{u}^s) \mathbf{n}^s \cdot \mathbf{n}^s - \Psi_h^s \mathbf{n}^s \cdot \mathbf{n}^s\|_e^2 \\
& \lesssim h \sum_{T \in \mathcal{T}_h(\Gamma^s)} h_T^{-1} \|D(\mathbf{u}^s) - \Psi_h^s\|_T^2 + h_T \|D(\mathbf{u}^s) - \Psi_h^s\|_{1,T}^2 \\
& \lesssim h^{2(r-1)} \|\mathbf{u}^s\|_{r,s}^2,
\end{aligned} \tag{4.14}$$

where $\mathcal{T}_h(\Gamma^s)$ is defined in (3.19). From the triangle inequality, (3.16), (4.9), (4.13), and (4.14), we get (4.10).

Finally, we will show (4.11) with the regularity $(\mathbf{u}^s, \mathbf{u}^d) \in [H^r(\Omega^s)]^N \times [H^{r-1}(\Omega^d)]^N$, $\nabla \cdot \mathbf{u}^d \in H^{r-1}(\Omega^d)$, and $p^i \in H^{r-1}(\Omega^i)$, $i = s, d$ for any $k \leq r \leq k+1$ with $k \geq 2$. For any $\psi_h \in V_h$, combining (2.1), (2.2), and (2.4) with Lemma 4.1, we have

$$\begin{aligned}
& (\mathbf{f}, \Pi_h \psi_h) \\
& = - (2\mu \nabla \cdot D(\mathbf{u}^s), \Pi_h^s \psi_h^s)_s + (\nabla p^s, \Pi_h^s \psi_h^s)_s + \mu (K^{-1} \mathbf{u}^d, \Pi_h^d \psi_h^d)_d + (\nabla p^d, \Pi_h^d \psi_h^d)_d \\
& = - (2\mu \nabla \cdot D(\mathbf{u}^s), \Pi_h^s \psi_h^s)_s + \mu (K^{-1} \mathbf{u}^d, \Pi_h^d \psi_h^d)_d + b(\Pi_h \psi_h, p) \\
& \quad + \langle p^s, \Pi_h^s \psi_h^s \cdot \mathbf{n}^s \rangle_\Gamma + \langle p^d, \Pi_h^d \psi_h^d \cdot \mathbf{n}^d \rangle_\Gamma \\
& = - (2\mu \nabla \cdot D(\mathbf{u}^s), \Pi_h^s \psi_h^s)_s + \mu (K^{-1} \mathbf{u}^d, \Pi_h^d \psi_h^d)_d + b(\Pi_h \psi_h, p) \\
& \quad + \langle 2\mu D(\mathbf{u}^s) \mathbf{n}^s \cdot \mathbf{n}^s, \Pi_h^s \psi_h^s \cdot \mathbf{n}^s \rangle_\Gamma + \langle p^d, \Pi_h^d \psi_h^d \cdot \mathbf{n}^d + \Pi_h^d \psi_h^d \cdot \mathbf{n}^d \rangle_\Gamma \\
& = - (2\mu \nabla \cdot D(\mathbf{u}^s), \Pi_h^s \psi_h^s)_s + \mu (K^{-1} \mathbf{u}^d, \Pi_h^d \psi_h^d)_d + b(\Pi_h \psi_h, p) \\
& \quad + \langle 2\mu D(\mathbf{u}^s) \mathbf{n}^s \cdot \mathbf{n}^s, \Pi_h^s \psi_h^s \cdot \mathbf{n}^s \rangle_\Gamma.
\end{aligned} \tag{4.15}$$

And from (3.10), (3.11), (3.12), and (3.13), it holds that

$$a(\mathbf{u}, \psi_h) = -2\mu (\nabla \cdot D(\mathbf{u}^s), \psi_h^s)_s + \mu (K^{-1} \mathbf{u}^d, \psi_h^d)_d + 2\mu \langle D(\mathbf{u}^s) \mathbf{n}^s \cdot \mathbf{n}^s, \psi_h^s \cdot \mathbf{n}^s \rangle_\Gamma. \tag{4.16}$$

With the help of (4.15) and (4.16) and noting $(1 - \Pi_h^d) \psi_h^d = 0$, it can be obtained

$$\begin{aligned}
& b(\psi_h, P_h p - p_h) \\
& = b(\psi_h, P_h p) + a(\mathbf{u}_h, \psi_h) - (\mathbf{f}, \Pi_h \psi_h) \\
& = a(\mathbf{u}, \psi_h) + b(\psi_h, P_h p) - (\mathbf{f}, \Pi_h \psi_h) - a(\mathbf{u} - \mathbf{u}_h, \psi_h) \\
& = (2\mu \nabla \cdot D(\mathbf{u}^s), \Pi_h^s \psi_h^s - \psi_h^s)_s + \langle 2\mu D(\mathbf{u}^s) \mathbf{n}^s \cdot \mathbf{n}^s, (\psi_h^s - \Pi_h^s \psi_h^s) \cdot \mathbf{n}^s \rangle_\Gamma \\
& \quad + b(\psi_h, P_h p - p) + b(\psi_h - \Pi_h \psi_h, p) - a(\mathbf{u} - \mathbf{u}_h, \psi_h),
\end{aligned} \tag{4.17}$$

where P_h is defined in (3.17). For the first two terms in (4.17), from Lemma 4.2, (4.13), and (4.14), it is easy to get

$$(2\mu \nabla \cdot D(\mathbf{u}^s), \Pi_h^s \psi_h^s - \psi_h^s)_s \lesssim \mu h^{r-1} \|\mathbf{u}^s\|_{r,s} \|\nabla \psi_h^s\|_s, \tag{4.18}$$

$$\langle 2\mu D(\mathbf{u}^s) \mathbf{n}^s \cdot \mathbf{n}^s, (\psi_h^s - \Pi_h^s \psi_h^s) \cdot \mathbf{n}^s \rangle_\Gamma \lesssim \mu h^{r-1} \|\mathbf{u}^s\|_{r,s} \|\nabla \psi_h^s\|_s. \tag{4.19}$$

Using the projection property and noting $\nabla \cdot \psi_h^d \in Q_h$, the third term in (4.17) holds

$$\begin{aligned}
b(\psi_h, P_h p - p) & = (\nabla \cdot \psi_h^s, (P_h p - p)^s)_s + (\nabla \cdot \psi_h^d, (P_h p - p)^d)_d \\
& \lesssim h^{r-1} \|p^s\|_{r-1,s} \|\nabla \psi_h\|_X.
\end{aligned} \tag{4.20}$$

For the fourth term in (4.17), with the help of the orthogonality property (4.1) and (4.2), the estimations (4.3) and (4.6), a discussion similar to (3.15) for $\inf_{\phi_h \in \Lambda_h} \|p^s - \phi_h\|_\Gamma$, and the

projection property, it can be obtained

$$\begin{aligned}
& b(\boldsymbol{\psi}_h - \Pi_h \boldsymbol{\psi}_h, p) \\
&= (\nabla \cdot (\boldsymbol{\psi}_h^s - \Pi_h \boldsymbol{\psi}_h^s), p^s)_s + (\nabla \cdot (\boldsymbol{\psi}_h^d - \Pi_h \boldsymbol{\psi}_h^d), p^d)_d \\
&= (\nabla \cdot (\boldsymbol{\psi}_h^s - \Pi_h \boldsymbol{\psi}_h^s), p^s)_s \\
&= -(\boldsymbol{\psi}_h^s - \Pi_h \boldsymbol{\psi}_h^s, \nabla p^s)_s + \langle (\boldsymbol{\psi}_h^s - \Pi_h \boldsymbol{\psi}_h^s) \cdot \mathbf{n}^s, p^s \rangle_\Gamma \\
&\lesssim \|\boldsymbol{\psi}_h^s - \Pi_h \boldsymbol{\psi}_h^s\|_s \sum_{T \in \mathcal{T}_h(\Omega^s)} \inf_{\Phi_h \in [P_{k-2}(T)]^N} \|\nabla p^s - \Phi_h\|_T \\
&\quad + \sum_{e \in \mathcal{E}_h(\Gamma)} \|\boldsymbol{\psi}_h^s - \Pi_h \boldsymbol{\psi}_h^s\|_e \inf_{\phi_h \in P_{k-1}(e)} \|p^s - \phi_h\|_e \\
&\lesssim h^{r-1} \|p^s\|_{r-1,s} \|\nabla \boldsymbol{\phi}_h^s\|_s.
\end{aligned} \tag{4.21}$$

Combining (4.17), (4.18), (4.19), (4.20), (4.21), and the boundedness of $a(\cdot, \cdot)$, the following estimate holds

$$\|P_h p - p_h\| \lesssim \sup_{\boldsymbol{\psi}_h \in V_h} \frac{b(\boldsymbol{\psi}_h, P_h p - p_h)}{\|\boldsymbol{\psi}_h\|_X} \lesssim (\mu h^{r-1} \|\mathbf{u}^s\|_{r,s}^2 + h^{r-1} \|p^s\|_{r-1,s}^2 + \mu \|u - u_h\|_X^2)^{1/2},$$

which implies (4.11) by triangle inequality $\|p - p_h\| \leq \|p - P_h p\| + \|P_h p - p_h\|$ and (4.10). \square

5 Numerical experiments

In this section, we present two numerical examples in two dimensions to validate the proposed methodology. Under a fixed viscosity, the first example compares the sensitivity of the error in classical method versus pressure-robust method to variations in the pressure field. On the contrary, under a fixed pressure, the second example shows the dependence of the error for classical method and pressure-robust method on perturbations of the viscosity. For both test cases, the Stokes equations are discretized using the \mathbf{P}_2^+ - P_1 finite element pair, while the Darcy problem employs the RT_1 - P_1 element. All these numerical examples have been implemented on a 2.4 GHz dual-core processor with 8 G RAM by MATLAB. The matrices were assembled with exact precision. The computation of the right-hand vectors and the approximation errors has been performed using a quadrature formula that is exact for polynomials up to the eighth degree. The left-division operator is applied directly for the resolution of the ensuing global linear systems.

5.1 Basis functions, degree of freedom, and computing $(\mathbf{f}, \Pi_h \boldsymbol{\psi}_h)$

The \mathbf{P}_2^+ and P_1 spaces utilize standard Lagrange basis functions supplemented with bubble functions. For the Raviart-Thomas (RT_1) elements, we use the Bernstein-Bézier local basis functions as detailed in [1]. The specific basis functions construction for any element T are given as follows:

$$\begin{aligned}
& \frac{1}{2|T|} (\lambda_2 |e_3| \mathbf{t}_3 - \lambda_3 |e_2| \mathbf{t}_2), \quad \frac{1}{2|T|} (\lambda_3 |e_1| \mathbf{t}_1 - \lambda_1 |e_3| \mathbf{t}_3), \quad \frac{1}{2|T|} (\lambda_1 |e_2| \mathbf{t}_2 - \lambda_2 |e_1| \mathbf{t}_1), \\
& \frac{1}{|T|} (\lambda_3 |e_2| \mathbf{t}_2 + \lambda_2 |e_3| \mathbf{t}_3), \quad \frac{1}{|T|} (\lambda_3 |e_1| \mathbf{t}_1 + \lambda_1 |e_3| \mathbf{t}_3), \quad \frac{1}{|T|} (\lambda_2 |e_1| \mathbf{t}_1 + \lambda_1 |e_2| \mathbf{t}_2), \\
& \frac{1}{|T|} (\lambda_1 \lambda_2 |e_3| \mathbf{t}_3 - \lambda_1 \lambda_3 |e_2| \mathbf{t}_2), \quad \frac{1}{|T|} (\lambda_1 \lambda_3 |e_2| \mathbf{t}_2 - \lambda_2 \lambda_3 |e_1| \mathbf{t}_1).
\end{aligned}$$

In this context, let e_j and \mathbf{t}_j ($j = 1, 2, 3$) represent the j -th edge and its corresponding unit tangent vector, respectively. The barycentric coordinates are denoted by $\{\lambda_j\}_{j=1}^3$, while $|T|$ and $|e_j|$ indicate the area (or length) of element T and edge e_j , respectively.

For the convenience of programming implementation, we will continue to provide the degree of freedom (*d.o.f*) for each finite element space [21]. Let S_p, S_s , and S_e represent the number of points, edges, and elements of $\mathcal{T}_h(\Omega^s)$, respectively. The *d.o.f* for any component function v_h in V_h^s with $k = 2$ is defined by point evaluation

$$\begin{cases} v_h(x_p^j), & j = 1, \dots, S_p, \\ v_h(x_m^j), & j = 1, \dots, S_s, \\ v_h(x_T) - \sum_{x_p^j \subset T} v_h(x_p^j) - \sum_{x_m^j \subset T} v_h(x_m^j), & T \in \mathcal{T}_h(\Omega^s). \end{cases}$$

where $\{x_p^j\}_{j=1}^{S_p}$, $\{x_m^j\}_{j=1}^{S_s}$, and $\{x_T\}_{T \in \mathcal{T}_h(\Omega^s)}$ are the enumerations of points in $\mathcal{T}_h(\Omega^s)$, midpoints of edges in $\mathcal{E}_h(\Omega^s)$, and centroid of elements in $\mathcal{T}_h(\Omega^s)$, respectively. The dimension of V_h^s is $2(S_p + S_s + S_e)$ in 2-dimensional case. If we expand the function v_h into the form of a linear combination of bases, the coefficients corresponding to the quadratic Lagrangian basis function are $v_h(x_p^j)$ and $v_h(x_m^j)$, respectively. The third point evaluation in above equation is the coefficients corresponding to the bubble basis functions ($27b_T$) in element T .

For the Darcy domain and $k = 2$, the finite element space V_h^d is the RT_1 with *d.o.f* defined by

$$\begin{cases} \int_e \mathbf{v}_h \cdot \mathbf{n} q_h, & q_h \text{ is the basis function of } P_1(e), e \in \mathcal{E}_h(\Omega^d), \\ \int_T \mathbf{v}_h \cdot \boldsymbol{\psi}_h, & \boldsymbol{\psi}_h \text{ is the basis function of } [P_0(T)]^2, T \in \mathcal{T}_h(\Omega^d). \end{cases}$$

for any function $\mathbf{v}_h \in V_h^d$. Let D_s and D_e represent the number of edges and elements of $\mathcal{T}_h(\Omega^d)$, respectively. The dimension of RT_1 is $2(D_s + D_e)$.

The pressure space Q_h with $k - 1 = 1$ is the first-order discontinuous Lagrange element. For any function q_h in Q_h , the *d.o.f* can be defined by

$$q_h(x_T^j), \quad j = 1, 2, 3, \text{ and } T \in \mathcal{T}_h,$$

where $\{x_T^j\}_{j=1}^3$ is an enumerations of vertices in T . The dimension of Q_h is $3N_e$, where N_e is the number of elements of \mathcal{T}_h .

When programming to implement pressure-robust method, only the right-hand side of the final linear system differs from classical method. In detail, the classical and pressure-robust methods to construct right-hand sides based on $(\mathbf{f}, \boldsymbol{\psi}_j)$ and $(\mathbf{f}, \Pi_h \boldsymbol{\psi}_j)$, respectively, where $\boldsymbol{\psi}_j$ is the basis functions in V_h . For the term $(\mathbf{f}, \boldsymbol{\psi}_j)$, a traditional quadrature formula is enough by obtaining the values of the integration points with respect to \mathbf{f} and $\boldsymbol{\psi}_j$, respectively. But for the term $(\mathbf{f}, \Pi_h \boldsymbol{\psi}_j)$, it becomes more complicated to get the values of the integration points with respect to $\Pi_h \boldsymbol{\psi}_j$. For any element $T \in \mathcal{T}_h$, let $\{\chi_\ell\}_{\ell=1}^8$ be the basis functions in RT_1 related to T . Then, we expand $\Pi_h \boldsymbol{\psi}_j|_T$ into the form of a linear combination of bases, i.e., $\Pi_h \boldsymbol{\psi}_j|_T = \sum_{\ell=1}^8 w_\ell \chi_\ell$. The coefficients w_ℓ will be determined by

$$\begin{cases} (\Pi_h \boldsymbol{\psi}_j \cdot \mathbf{n}, \phi_h)_e = (\boldsymbol{\psi}_j \cdot \mathbf{n}, \phi_h)_e, & \forall \phi_h \in P_1(e), e \subset \partial T, \\ (\Pi_h \boldsymbol{\psi}_j, \phi_h)_T = (\boldsymbol{\psi}_j, \phi_h)_T, & \forall \phi_h \in [P_0(T)]^2. \end{cases}$$

5.2 Example for different pressure

This example is taken from [6] and has been modified with an adjustable parameter γ to compares the error behavior of pressure-robust method with classical method under varying pressure. The domain is $\Omega = (0, 1) \times (0, 1)$ with interface $y = 0.5$, i.e. $\Omega^s = (0, 1) \times (0.5, 1)$ and

$\Omega^d = (0, 1) \times (0, 0.5)$. We consider the coupled system with the following exact solution

$$\begin{aligned} \mathbf{u}^s &= \left[-\frac{e^{\frac{y}{2}} \sin(\pi x)}{2\pi^2}, \frac{e^{\frac{y}{2}} \cos(\pi x)}{\pi} \right]^t, & p^s &= -\frac{\gamma e^{\frac{y}{2}} \cos(\pi x)}{\pi}, \\ \mathbf{u}^d &= \left[-2e^{\frac{y}{2}} \sin(\pi x), \frac{e^{\frac{y}{2}} \cos(\pi x)}{\pi} \right]^t, & p^d &= -\frac{(\gamma + 1)e^{\frac{y}{2}} \cos(\pi x)}{\pi}. \end{aligned}$$

In (2.6), the constant $\frac{\alpha_1}{\sqrt{\kappa_1}} = (1 + 4\pi^2)/2$ can be directly derived from the exact solutions of the system. Following this approach, we also obtain the functional expressions for \mathbf{f} and \mathbf{g} . To evaluate the performance of both methods, we fix $\mu = 1$ and $K = 10^{-4}$ while selecting γ values from the geometric sequence $\{1, 10, 10^2, 10^3, 10^4, 10^5\}$.

As demonstrated in Table 5.1, a comprehensive comparison reveals that while both the classical and pressure-robust methods achieve the theoretically predicted convergence orders, their error behaviors diverge significantly with increasing γ . At $\gamma = 1$, both methods exhibit nearly identical performance in both error metrics and computational time. However, for $\gamma = 10^5$, the classical method demonstrates a substantially larger velocity error compared to the pressure-robust method, despite comparable computational costs. This discrepancy is further corroborated by the component-wise error decomposition in Figures 5.1, 5.2, and 5.3, which highlight that the elevated velocity error in the classical method predominantly originates from the Stokes domain. These observations collectively confirm that the velocity error of the pressure-robust method remains decoupled from pressure influences, whereas the classical method's velocity error exhibits pressure-dependent behavior.

Figure 5.3 reveals an additional critical feature: both the velocity and pressure errors of the classical method, along with the pressure error of the pressure-robust method, display a distinct piecewise growth pattern with respect to γ . Specifically, errors increase gradually for $\gamma \in [1, 10^2]$ but accelerate markedly for $\gamma \in [10^2, 10^5]$. This bifurcated trend aligns precisely with the theoretical framework established in Theorems 3.1 and 4.1. As indicated by the error estimates in (3.8), (3.9), and (4.11), all three error components adopt a unified parametric form $C_1 + \gamma C_2$, where C_1 and C_2 represent γ -independent constants. This formulation explains the observed transition between error regimes as γ exceeds 10^2 .

5.3 Example for different viscosity

This example from reference [13] compares the error behavior of pressure-robust method with classical method under varying viscosity. The Stokes and Darcy domains are $\Omega^s = (0, \pi) \times (0, \pi)$ and $\Omega^d = (0, \pi) \times (-\Omega, 0)$, respectively. The interface is $\Gamma : y = 0$. The exact solution are as follows

$$\begin{aligned} \mathbf{u}^s &= [2 \sin y \cos y \cos x, (\sin^2 y - 2) \sin x]^t, & p^s &= \sin x \sin y + 1669/(87\pi^2), \\ \mathbf{u}^d &= [-(e^y - e^{-y}) \cos x, -(e^y + e^{-y}) \sin x]^t, & p^d &= (e^y - e^{-y}) \sin x + 1669/(87\pi^2). \end{aligned}$$

This additive constant $1669/(87\pi^2)$ ensures the condition $p \in L_0^2(\Omega)$ holds. Under the tangential constraint $\mathbf{u}^s \cdot \boldsymbol{\tau}_{1|\Gamma} = -2D(\mathbf{u}^s)\mathbf{n}^s \cdot \boldsymbol{\tau}_{1|\Gamma} = 0$, the coefficient α_1 in (2.5) admits any bounded value. Implementing with $K = 10^{-4}$, we conduct a viscosity study ($\mu \in [10^{-6}, 10^6]$) to quantify *d.o.f*-convergence relationships and error performance contrasting classical and pressure-robust method.

Focus on the error performance of velocity. With viscosity coefficients $\mu = 10^{-6}, 1, 10^6$, Table 5.2 demonstrate that both methods attain theoretically predicted convergence rates, while their error magnitudes exhibit different dependence on viscosity variations. In detail, when $\mu = 1$ or 10^6 , Table 5.2 shows the errors of classical and pressure-robust method have almost the same performance. However, when $\mu = 10^{-6}$, classical method are affected by the viscosity, and the error in velocity is several orders of magnitude larger than that of pressure-robust method.

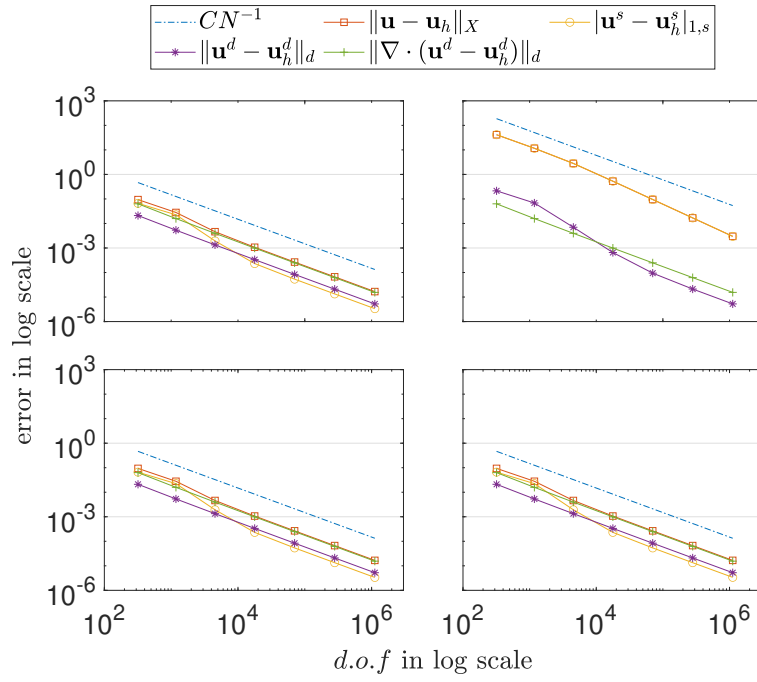


FIGURE 5.1. Convergence rates of velocity for classical method (top) and pressure-robust method (bottom) with $\gamma = 1$ (left) and 10^5 (right), respectively, in Example 5.2.

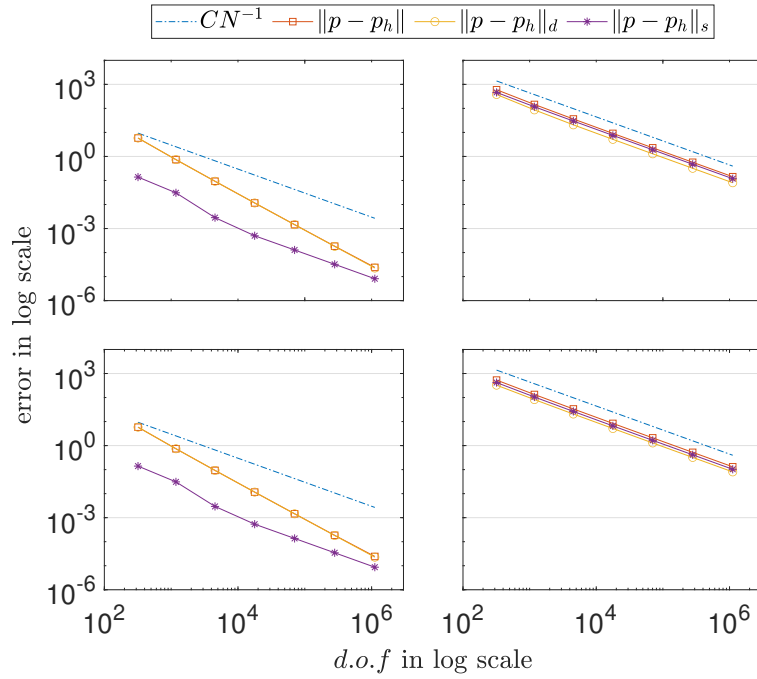


FIGURE 5.2. Convergence rates of pressure for classical method (top) and pressure-robust method (bottom) with $\gamma = 1$ (left) and 10^5 (right), respectively, in Example 5.2.

TABLE 5.1. The comparison of error and time cost between classical method and pressure-robust method in Example 5.2.

	$d.o.f$	$\ \mathbf{u} - \mathbf{u}_h\ _X$	order	$\ p - p_h\ $	order	time(s)
classical method $\gamma = 1$	319	9.383E-2	—	5.836E0	—	1.829
	1179	2.807E-2	0.923	7.385E-1	1.581	0.439
	4531	4.613E-3	1.341	9.273E-2	1.541	0.342
	17763	1.071E-3	1.068	1.159E-2	1.521	0.621
	70339	2.669E-4	1.009	1.453E-3	1.508	1.619
	279939	6.674E-5	1.003	1.839E-4	1.496	11.942
	1116931	1.668E-5	1.001	2.411E-5	1.468	64.015
pressure-robust method $\gamma = 1$	319	9.375E-2	—	5.836E0	—	2.909
	1179	2.798E-2	0.924	7.386E-1	1.581	0.582
	4531	4.605E-3	1.340	9.273E-2	1.541	0.815
	17763	1.071E-3	1.067	1.159E-2	1.521	1.212
	70339	2.669E-4	1.009	1.454E-3	1.508	2.643
	279939	6.674E-5	1.003	1.843E-4	1.495	14.563
	1116931	1.668E-5	1.001	2.430E-5	1.464	75.289
classical method $\gamma = 10^5$	319	4.153E1	—	5.985E2	—	2.464
	1179	1.161E1	0.974	1.458E3	1.079	0.509
	4531	2.804E0	1.055	3.627E1	1.033	0.489
	17763	5.292E-1	1.220	9.120E0	1.010	1.239
	70339	9.491E-2	1.248	2.287E0	1.004	2.084
	279939	1.684E-2	1.251	5.728E-1	1.002	13.666
	1116931	2.980E-3	1.251	1.433E-1	1.001	66.332
pressure-robust method $\gamma = 10^5$	319	9.375E-2	—	5.325E2	—	2.052
	1179	2.798E-2	0.924	1.338E2	1.056	0.575
	4531	4.605E-3	1.340	3.351E1	1.028	0.799
	17763	1.071E-3	1.067	8.382E-1	1.014	1.219
	70339	2.669E-4	1.009	2.095E-1	1.007	2.646
	279939	6.674E-5	1.003	5.239E-2	1.003	14.371
	1116931	1.669E-5	1.001	1.309E-2	1.001	73.944

The streamline comparison in Figure 5.4 also reflects this point. This numerical phenomenon is completely consistent with theoretical analysis in (3.8) and (4.10), i.e. the error of classical method demonstrate an inverse functional dependence on the viscosity and the error of pressure-robust method is independent of viscosity. For a more intuitive comparison of convergence behavior and error components between the two methods, Figure 5.5 comprehensively presents both total errors and their constituent elements. With the $d.o.f$ fixed at 8931, Figure 5.7 subsequently demonstrates the error evolution as a function of the parameter μ .

Turning gaze towards the error of pressure, Table 5.2 reveals both methods maintain comparable error magnitudes and demonstrate analogous convergence characteristics with varying viscosity. A more intuitive comparison is presented in Figure 5.6. With the $d.o.f$ fixed at 8931, Figure 5.7 demonstrates the error behavior under varying values of the parameter μ . For $\mu \in [10^{-6}, 10^{-3}]$, the error remains nearly constant, indicating negligible dependence on μ in this regime. In contrast, as μ increases from 10^{-2} to 10^6 , the error grows linearly with a consistent slope. This trend aligns with the theoretical error bounds derived in (3.9) and (4.11), which can be concisely expressed as $\|p - p_h\| \lesssim \mu C_u + C_p$, where C_u and C_p are problem-dependent constants associated with the velocity and pressure approximations, respectively.

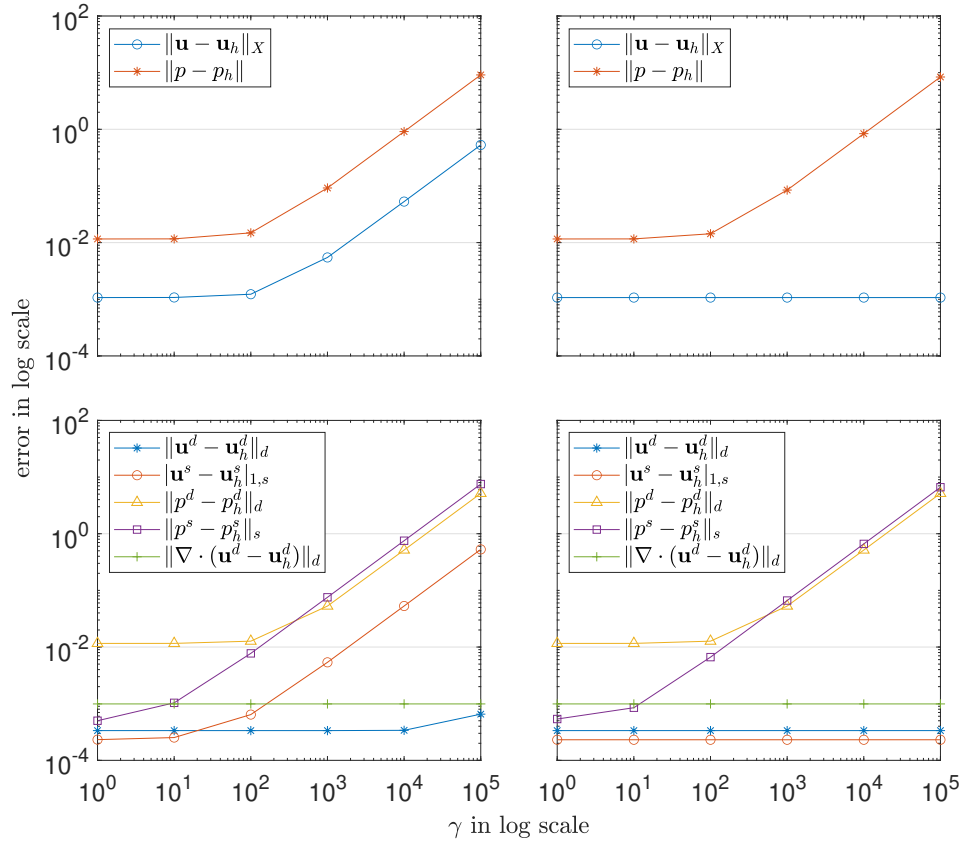


FIGURE 5.3. Total errors (top) and component errors (bottom) for classical method (left) and pressure-robust method (right) with $d.o.f = 17763$ in Example 5.2.

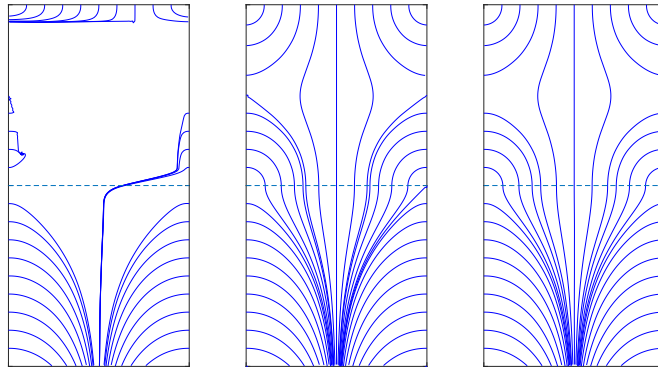


FIGURE 5.4. Streamlines of velocity for classical method (left), exact solution (middle), and pressure-robust method (right) with $\mu = 10^{-6}$ and $d.o.f = 8931$, in Example 5.3.

TABLE 5.2. The comparison of error and time cost between classical method and pressure-robust method in Example 5.3.

	$d.o.f$	$\ \mathbf{u} - \mathbf{u}_h\ _X$	order	$\ p - p_h\ $	order	time(s)
classical method $\mu = 10^{-6}$	167	3.203E4	–	2.526E0	–	1.530
	603	7.177E3	1.164	6.844E-1	1.017	0.397
	2291	1.327E3	1.264	1.749E-1	1.021	0.239
	8931	2.367E2	1.267	4.398E-2	1.014	0.342
	35267	4.183E1	1.261	1.101E-2	1.008	0.923
	140163	7.392E0	1.256	2.753E-3	1.004	5.473
	558851	1.306E0	1.253	6.885E-4	1.002	23.912
pressure-robust method $\mu = 10^{-6}$	167	5.624E0	–	2.524E0	–	1.726
	603	1.546E0	1.005	6.837E-1	1.017	0.502
	2291	4.088E-1	0.996	1.747E-1	1.022	0.637
	8931	1.053E-1	0.996	4.393E-2	1.014	0.784
	35267	2.682E-2	0.996	1.099E-2	1.008	1.320
	140163	6.753E-3	0.999	2.750E-3	1.004	6.098
	558851	1.694E-3	0.999	6.877E-4	1.002	26.164
classical method $\mu = 1$	167	5.615E0	–	7.171E3	–	1.529
	603	1.542E0	1.006	1.039E3	1.504	0.354
	2291	4.081E-1	0.995	1.370E2	1.517	0.259
	8931	1.053E-1	0.995	1.741E1	1.516	0.336
	35267	2.682E-2	0.995	2.186E0	1.510	0.878
	140163	6.753E-3	0.999	2.737E-1	1.505	4.468
	558851	1.692E-3	1.000	3.430E-2	1.501	19.310
pressure-robust method $\mu = 1$	167	5.624E0	–	7.171E3	–	1.830
	603	1.546E0	1.005	1.039E3	1.504	0.516
	2291	4.088E-1	0.996	1.370E2	1.517	0.606
	8931	1.053E-1	0.996	1.741E1	1.516	0.859
	35267	2.682E-2	0.996	2.186E0	1.510	1.429
	140163	6.753E-3	0.999	2.737E-1	1.505	5.863
	558851	1.692E-3	1.000	3.430E-2	1.501	24.965
classical method $\mu = 10^6$	167	5.615E0	–	7.171E9	–	1.218
	603	1.542E0	1.006	1.039E9	1.504	0.268
	2291	4.081E-1	0.995	1.370E8	1.517	0.233
	8931	1.053E-1	0.995	1.741E7	1.516	0.345
	35267	2.682E-2	0.995	2.186E6	1.510	0.895
	140163	6.753E-3	0.999	2.737E5	1.505	4.830
	558851	1.692E-3	1.000	3.430E4	1.501	21.470
pressure-robust method $\mu = 10^6$	167	5.624E0	–	7.171E9	–	1.830
	603	1.546E0	1.005	1.039E9	1.504	0.516
	2291	4.088E-1	0.996	1.370E8	1.517	0.606
	8931	1.053E-1	0.996	1.741E7	1.516	0.859
	35267	2.682E-2	0.996	2.186E6	1.510	1.429
	140163	6.753E-3	0.999	2.737E5	1.505	5.863
	558851	1.692E-3	1.000	3.430E4	1.501	24.965

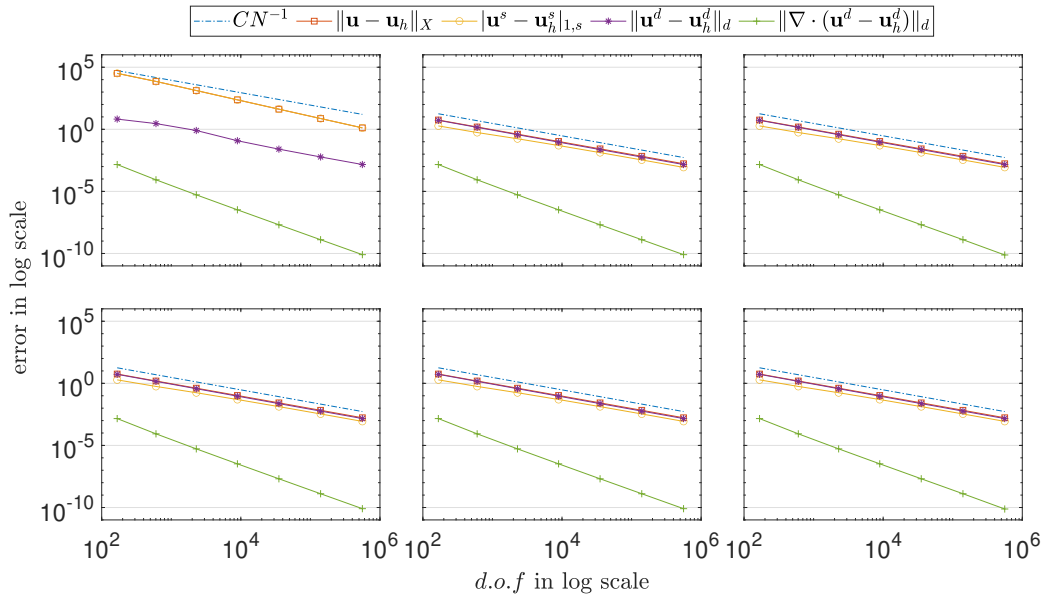


FIGURE 5.5. Convergence rates of velocity for classical method (top) and pressure-robust method (bottom) with $\mu = 10^{-6}$ (left), 1 (middle), and 10^6 (right), respectively, in Example 5.3.

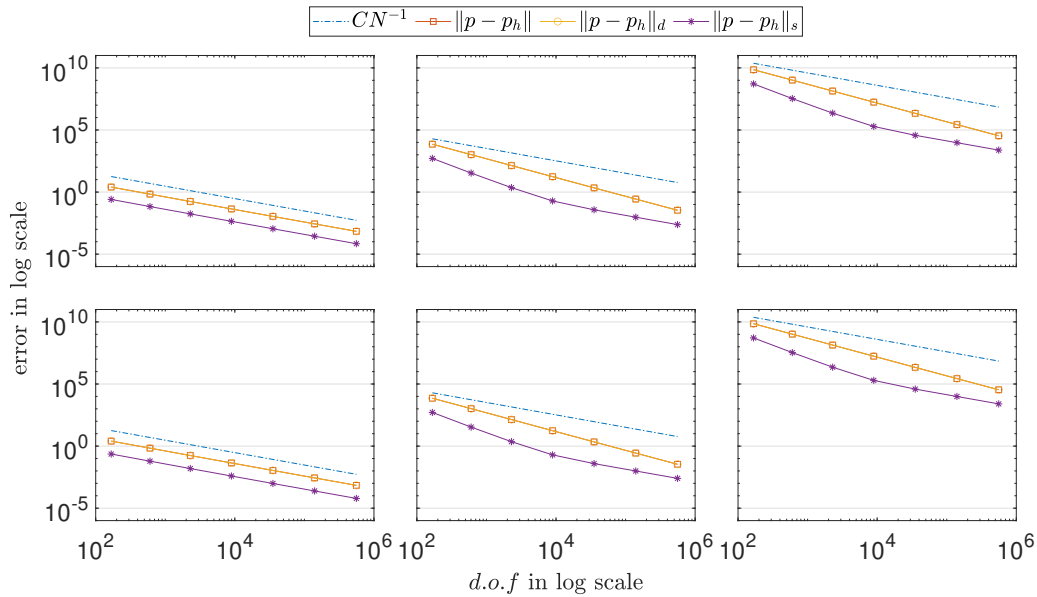


FIGURE 5.6. Convergence rates of pressure for classical method (top) and pressure-robust method (bottom) with $\mu = 10^{-6}$ (left), 1 (middle), and 10^6 (right), respectively, in Example 5.3.

6 Conclusion

This study presents a comprehensive analysis of pressure-robust mixed FEM for the Stokes-Darcy coupled problem, addressing critical gaps in existing methodologies. By decoupling velocity and pressure errors, we reveal how classical method incur pressure-dependent consistency errors, leading to velocity inaccuracies proportional to pressure and inversely proportional to

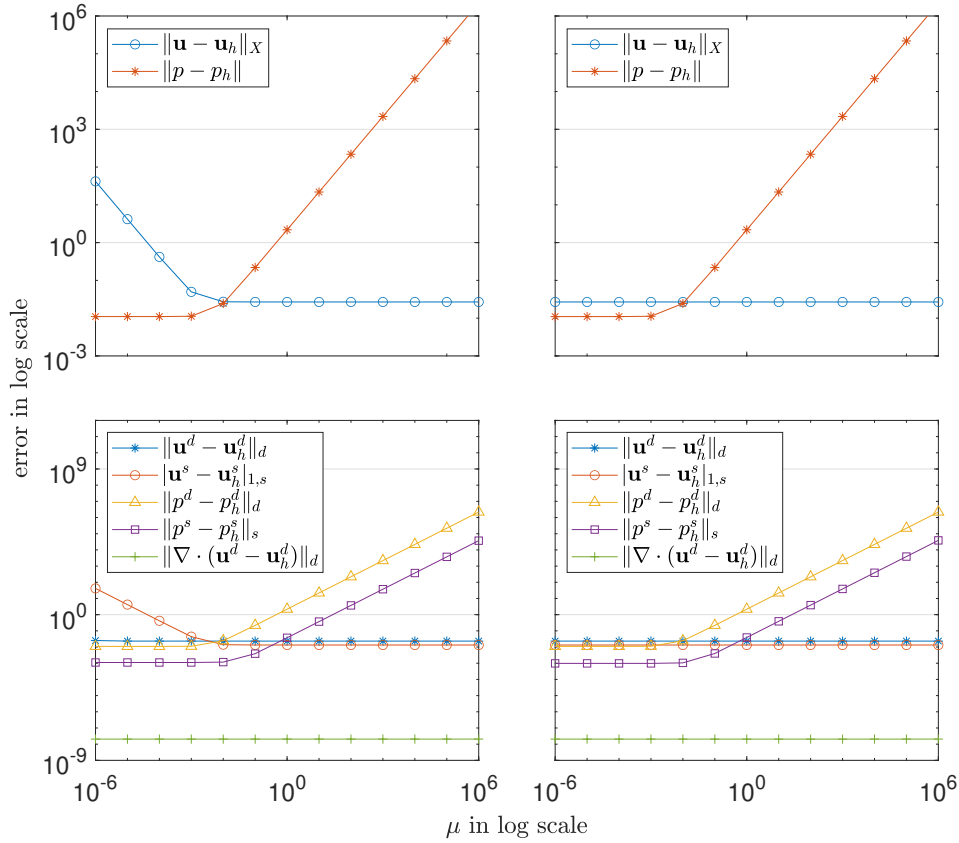


FIGURE 5.7. Total errors (top) and component errors (bottom) for classical method (left) and pressure-robust method (right) with $d.o.f = 8931$ in Example 5.3.

viscosity. The proposed pressure-robust method, enhanced by divergence-free reconstruction operators, effectively eliminates these errors by enforcing exact divergence constraints and interface continuity. Numerical experiments corroborate theoretical findings, demonstrating the superiority of the pressure-robust approach in high-pressure or low-viscosity regimes. Notably, our framework overcomes the limitations of recent studies confined to low-order or two-dimensional cases, demonstrating adaptability to higher-order and three-dimensional settings. Future work could extend this approach to continuous pressure finite element spaces, time-dependent problems, or nonlinear fluid-structure interactions, thereby further enhancing the robustness and efficiency of coupled multi-physics simulations.

Acknowledgments

The work of J. Zhang is supported by the National Natural Science Foundation of China (No. 12301469) and the Natural Science Foundation of Jiangsu Province (No. BK20210540).

Appendix A.

The proof of Lemma 3.1. Let Υ_1^s be the interpolation operator from V^s to $M_1^s = \{\mathbf{v}_h^s \in V^s \mid \mathbf{v}_h^s|_T \in [P_1(T)]^N, T \in \mathcal{T}_h(\Omega^s)\} \subset V_1^s$. For any $\mathbf{v}^s \in V^s$, we then have

$$\sum_{T \in \mathcal{T}_h(\Omega^s)} h_T^{2m-2} |\mathbf{v}^s - \Upsilon_1^s \mathbf{v}^s|_{m,T}^2 \lesssim \|\mathbf{v}^s\|_{1,s}^2, \quad m = 0, 1. \quad (\text{A.1})$$

Define the operator Υ_2^s from V^s to V_1^s by:

$$\begin{cases} \Upsilon_2^s \mathbf{v}^s(x) = 0, & \forall \text{ node } x \text{ of } \mathcal{T}_h(\Omega^s), \\ \int_f (\Upsilon_2^s \mathbf{v}^s - \mathbf{v}^s) \cdot \mathbf{n} = 0, & \forall \text{ side (or face) } f \text{ of } \mathcal{T}_h(\Omega^s). \end{cases} \quad (\text{A.2})$$

For any $T \in \mathcal{T}_h(\Omega^s)$, it is clear $\Upsilon_2^s \mathbf{v}^s|_T = \sum_{j=1}^{N+1} \alpha_j \mathbf{p}_j$ with $\alpha_j = (\int_{f_j} \mathbf{v}^s \cdot \mathbf{n}_j) / (\int_{f_j} \prod_{l=1}^N \lambda_{jl})$, where f_j is the j -th side (or face) of T .

Let \tilde{T} be a fixed reference element with $h_{\tilde{T}} = 1$. For any $T \in \mathcal{T}_h(\Omega^s)$, there exists an invertible affine mapping G such that $T = G(\tilde{T})$. For each $\psi : T \rightarrow \mathbb{R}$, define $\tilde{\psi} = \psi \circ G$. Analogous definitions are given for the functions defined on the sub-simplices of T and \tilde{T} . From the scale argument, it is clear that

$$|\mathbf{p}_j|_{m,T} = h_T^{N/2-m} |\tilde{\mathbf{p}}_j|_{m,\tilde{T}}, \quad \int_{f_j} \prod_{l=1}^N \lambda_{jl} = h_T^{N-1} \int_{\tilde{f}_j} \prod_{l=1}^N \tilde{\lambda}_{jl}.$$

And combining with trace theorem, we have

$$\begin{aligned} \int_{f_j} \mathbf{v}^s \cdot \mathbf{n}_j &= h_T^{N-1} \int_{\tilde{f}_j} \tilde{\mathbf{v}}^s \cdot \tilde{\mathbf{n}}_j \lesssim h_T^{N-1} \|\tilde{\mathbf{v}}^s\|_{0,\tilde{f}_j} \lesssim h_T^{N-1} \|\tilde{\mathbf{v}}^s\|_{1,\tilde{T}} \\ &\lesssim h_T^{N-1} (h_T^{-N/2} \|\mathbf{v}^s\|_{0,T} + h_T^{1-N/2} |\mathbf{v}^s|_{1,T}) \\ &= h_T^{N/2-1} \|\mathbf{v}^s\|_{0,T} + h_T^{N/2} |\mathbf{v}^s|_{1,T}, \end{aligned}$$

where $|\tilde{\mathbf{p}}_j|_{m,\tilde{T}}$ and $\int_{\tilde{f}_j} \prod_{l=1}^N \tilde{\lambda}_{jl}$ are constants independent of T . Thus, it can be derived that

$$\begin{aligned} |\alpha_j| &\lesssim h_T^{-N/2} \|\mathbf{v}^s\|_{0,T} + h_T^{1-N/2} |\mathbf{v}^s|_{1,T}, \\ |\Upsilon_2^s \mathbf{v}^s|_{0,T} &= \left| \sum_{j=1}^{N+1} \alpha_j \mathbf{p}_j \right|_{0,T} \lesssim \|\mathbf{v}^s\|_{0,T} + h_T |\mathbf{v}^s|_{1,T}, \end{aligned} \quad (\text{A.3})$$

$$|\Upsilon_2^s \mathbf{v}^s|_{1,T} = \left| \sum_{j=1}^{N+1} \alpha_j \mathbf{p}_j \right|_{1,T} \lesssim h_T^{-1} \|\mathbf{v}^s\|_{0,T} + |\mathbf{v}^s|_{1,T}. \quad (\text{A.4})$$

From integration by parts and the definition of Υ_2^s in (A.2), it is easy to obtain

$$\int_T \nabla \cdot (\Upsilon_2^s \mathbf{v}^s - \mathbf{v}^s) = \int_{\partial T} (\Upsilon_2^s \mathbf{v}^s - \mathbf{v}^s) \cdot \mathbf{n} = 0. \quad (\text{A.5})$$

Using the interpolation properties of Υ_1^s in (A.1) and the estimates of Υ_2^s in (A.3) and (A.4), we have

$$\|\Upsilon_1^s \mathbf{v}^s\|_{1,\Omega^s} \leq \|\Upsilon_1^s \mathbf{v}^s - \mathbf{v}^s\|_{1,s} + \|\mathbf{v}^s\|_{1,s} \lesssim \|\mathbf{v}^s\|_{1,s}, \quad (\text{A.6})$$

and

$$\begin{aligned} \|\Upsilon_2^s (1 - \Upsilon_1^s) \mathbf{v}^s\|_{1,s}^2 &= \sum_{T \in \mathcal{T}_h(\Omega^s)} \|\Upsilon_2^s (1 - \Upsilon_1^s) \mathbf{v}^s\|_{1,T}^2 \\ &\lesssim \sum_{T \in \mathcal{T}_h(\Omega^s)} h_T^{-2} \|(1 - \Upsilon_1^s) \mathbf{v}^s\|_{0,T}^2 + |(1 - \Upsilon_1^s) \mathbf{v}^s|_{1,T}^2 \\ &\lesssim \|\mathbf{v}^s\|_{1,s}^2. \end{aligned} \quad (\text{A.7})$$

Setting $\Upsilon_h^s \mathbf{v}^s = \Upsilon_2^s(\mathbf{v}^s - \Upsilon_1^s \mathbf{v}^s) + \Upsilon_1^s \mathbf{v}^s$ and with the help of (A.5), (A.6), and (A.7), we can get

$$\begin{aligned} \int_{\Omega^s} \nabla \cdot (\Upsilon_h^s \mathbf{v}^s) &= \int_{\Omega^s} \nabla \cdot (\Upsilon_2^s(\mathbf{v}^s - \Upsilon_1^s \mathbf{v}^s)) + \int_{\Omega^s} \nabla \cdot (\Upsilon_1^s \mathbf{v}^s) \\ &= \int_{\Omega^s} \nabla \cdot (\mathbf{v}^s - \Upsilon_1^s \mathbf{v}^s) + \int_{\Omega^s} \nabla \cdot (\Upsilon_1^s \mathbf{v}^s) \\ &= \int_{\Omega^s} \nabla \cdot \mathbf{v}^s, \end{aligned}$$

and

$$\|\Upsilon_h^s \mathbf{v}^s\|_{1,s} \leq \|\Upsilon_2^s(\mathbf{v}^s - \Upsilon_1^s \mathbf{v}^s)\|_{1,s} + \|\Upsilon_1^s \mathbf{v}^s\|_{1,s} \lesssim \|\mathbf{v}^s\|_{1,s}.$$

Thus, we complete the proof. \square

Appendix B.

The proof of Lemma 4.1. For any $\mathbf{v}_h \in V_h$, we have $\mathbf{v}_h^s = 0$ on Γ^s , and $\mathbf{v}_h^d \cdot \mathbf{n}^d = 0$ on Γ^d , and $\langle \mathbf{v}_h^s \cdot \mathbf{n}^s + \mathbf{v}_h^d \cdot \mathbf{n}^d, q_h \rangle_e = 0$ for any $q_h \in P_{k-1}(e), e \subset \Gamma$. From (4.2) and noting that $\Pi_h \mathbf{v}_h \cdot \mathbf{n} \in P_{k-1}(e), e \subset \partial T$ for any $T \in \mathcal{T}_h$, we get $\Pi_h^s \mathbf{v}_h^s \cdot \mathbf{n}^s = 0$ on Γ^s , $\Pi_h^d \mathbf{v}_h^d \cdot \mathbf{n}^d = 0$ on Γ^d , and $\Pi_h^s \mathbf{v}_h^s \cdot \mathbf{n}^s + \Pi_h^d \mathbf{v}_h^d \cdot \mathbf{n}^d = 0$ on Γ .

Moreover, For any $\mathbf{v}_h \in V_h(0)$, from $\nabla \cdot (\Pi_h \mathbf{v}_h)_T \in P_{k-1}(T)$ and $(\nabla \cdot (\Pi_h \mathbf{v}_h), 1) = (\Pi_h \mathbf{v}_h \cdot \mathbf{n}, 1)_{\partial \Omega} = 0$, we have $\nabla \cdot (\Pi_h \mathbf{v}_h) \subset Q_h$. And, from the integral by part, (4.1), (4.2), and $b(\mathbf{v}_h, q_h) = 0$ for any $q_h \in Q_h$, it holds

$$\begin{aligned} (\nabla \cdot (\Pi_h \mathbf{v}_h), q_h) &= \sum_{T \in \mathcal{T}_h} (\nabla \cdot (\Pi_h^{i_T} \mathbf{v}_h), q_h)_T = - \sum_{T \in \mathcal{T}_h} (\Pi_h^{i_T} \mathbf{v}_h, \nabla q_h)_T + \langle \Pi_h^{i_T} \mathbf{v}_h \cdot \mathbf{n}, q_h \rangle_{\partial T} \\ &= - \sum_{T \in \mathcal{T}_h} (\mathbf{v}_h, \nabla q_h)_T + \langle \mathbf{v}_h \cdot \mathbf{n}, q_h \rangle_{\partial T} = \sum_{T \in \mathcal{T}_h} (\nabla \cdot \mathbf{v}_h, q_h)_T = 0. \end{aligned}$$

According to $T \in \Omega^s$ or Ω^d , i_T takes values of s or d . The above analysis means $\nabla \cdot (\Pi_h \mathbf{v}_h) = 0$. \square

References

- [1] Mark Ainsworth, Gaëlle Andriamaro, and Oleg Davydov. A Bernstein–Bézier basis for arbitrary order Raviart–Thomas finite elements. *Constructive Approximation*, 41:1–22, 2015.
- [2] Daniele Boffi, Franco Brezzi, and Michel Fortin. *Mixed finite element methods and applications*. Springer Series in Computational Mathematics. Springer Berlin Heidelberg, 2013.
- [3] Franco Brezzi and Michel Fortin. *Mixed and hybrid finite element methods*, volume 15 of *Springer Series in Computational Mathematics*. Springer New York, 1991.
- [4] Pei Cao and Jinru Chen. An extended finite element method for coupled Darcy–Stokes problems. *International Journal for Numerical Methods in Engineering*, 123(19):4586–4615, 2022.
- [5] Bernardo Cockburn, Guido Kanschat, and Dominik Schötzau. A note on discontinuous galerkin divergence-free solutions of the navier stokes equations. *Journal of Scientific Computing*, 31:61–73, 2007.
- [6] M.R. Correa and A.F.D. Loula. A unified mixed formulation naturally coupling Stokes and Darcy flows. *Computer Methods in Applied Mechanics and Engineering*, 198(33-36):2710–2722, 2009.
- [7] Marco Discacciati, Edie Miglio, and Alfio Quarteroni. Mathematical and numerical models for coupling surface and groundwater flows. *Applied Numerical Mathematics*, 43(1-2):57–74, 2002.
- [8] Marco Discacciati and Alfio Quarteroni. Convergence analysis of a subdomain iterative method for the finite element approximation of the coupling of Stokes and Darcy equations. *Computing and Visualization in Science*, 6(2-3):93–103, 2004.
- [9] Richard S. Falk and Michael Neilan. Stokes Complexes and the construction of stable finite elements with pointwise mass conservation. *SIAM Journal on Numerical Analysis*, 51:1308–1326, 2013.
- [10] Gabriel N. Gatica, Salim Meddahi, and Ricardo Oyarzúa. A conforming mixed finite-element method for the coupling of fluid flow with porous media flow. *IMA Journal of Numerical Analysis*, 29(1):86–108, 2008.
- [11] Gabriel Gatica, Ricardo Oyarzúa, and Francisco-Javier Sayas. Analysis of fully-mixed finite element methods for the Stokes–Darcy coupled problem. *Mathematics of Computation*, 80(276):1911–1948, 2011.
- [12] Johnny Guzmán and Michael Neilan. Conforming and divergence-free Stokes elements in three dimensions. *IMA Journal of Numerical Analysis*, 34:1489–1508, 2014.

- [13] Jiwei Jia, Lin Yang, and Qilong Zhai. The pressure-robust weak Galerkin finite element method for Stokes-Darcy problem. *arXiv:2408.05658*, 2024.
- [14] Volker John, Alexander Linke, Christian Merdon, Michael Neilan, and Leo G. Rebholz. On the divergence constraint in mixed finite element methods for incompressible flows. *SIAM Review*, 59:492–544, 2017.
- [15] William J. Layton, Friedhelm Schieweck, and Ivan Yotov. Coupling fluid flow with porous media flow. *SIAM Journal on Numerical Analysis*, 40:2195–2218, 2002.
- [16] Philip L. Lederer, Alexander Linke, Christian Merdon, and Joachim Schöberl. Divergence-free reconstruction operators for pressure-robust Stokes discretizations with continuous pressure finite elements. *SIAM Journal on Numerical Analysis*, 55:1291–1314, 2017.
- [17] Jingshi Li, Jiachuan Zhang, and Ran Zhang. Pressure-robustness in Stokes-Darcy Optimal Control Problem with reconstruction operator. *arXiv:2502.16501*, 2025.
- [18] Alexander Linke. A divergence-free velocity reconstruction for incompressible flows. *Comptes Rendus. Mathématique*, 350(17–18):837–840, 2012.
- [19] Alexander Linke, Gunar Matthies, and Lutz Tobiska. Robust arbitrary order mixed finite element methods for the incompressible Stokes equations with pressure independent velocity errors. *ESAIM: Mathematical Modelling and Numerical Analysis*, 50(1):289–309, 2016.
- [20] Alexander Linke, Christian Merdon, and Michael Neilan. Pressure-robustness in quasi-optimal a priori estimates for the Stokes problem. *Electronic Transactions on Numerical Analysis*, 52:281–294, 2020.
- [21] Anders Logg, Kent-Andre Mardal, and Garth Wells. *Automated solution of differential equations by the finite element method: The FEniCS Book*. Springer Berlin Heidelberg, 2012.
- [22] Deyong Lv and Hongxing Rui. A pressure-robust mixed finite element method for the coupled Stokes–Darcy problem. *Journal of Computational and Applied Mathematics*, 436:115444, January 2024.
- [23] P. A. Raviart and J. M. Thomas. *A mixed finite element method for 2-nd order elliptic problems. Mathematical Aspects of Finite Element Methods. Lecture Notes in Mathematics, vol 606*. Springer Berlin Heidelberg, 1977,292–315.
- [24] Béatrice Rivière and Ivan Yotov. Locally conservative coupling of Stokes and Darcy flows. *SIAM Journal on Numerical Analysis*, 42(5):1959–1977, 2005.
- [25] Danail Vassilev, ChangQing Wang, and Ivan Yotov. Domain decomposition for coupled Stokes and Darcy flows. *Computer Methods in Applied Mechanics and Engineering*, 268:264–283, 2014.
- [26] Junping Wang and Xiu Ye. New finite element methods in computational fluid dynamics by H(div) elements. *SIAM Journal on Numerical Analysis*, 45:1269–1286, 2007.
- [27] Jing Wen, Jian Su, Yinnian He, and Hongbin Chen. A discontinuous Galerkin method for the coupled Stokes and Darcy problem. *Journal of Scientific Computing*, 85(2):26, 2020.